Data Analysis For Bark and Leaf Reflectance Measurements

J.H. Gruninger, D.C. Robertson and M.M. Pervaiz

Spectral Sciences, Inc.
Burlington, MA

PL-TR-92-2151

SWOE Report 92-6

June 1992

Data Analysis For Bark and Leaf Reflectance Measurements

J.H. Gruninger, D.C. Robertson
and M.M. Pervaiz

Spectral Sciences, Inc.
Burlington, MA

PL-TR-92-2151

SWOE Report 92-6
June 1992

FOREWORD

SWOE Report 92-6, June 1992, was prepared by Dr. J.H. Gruninger, Dr. D.C. Robertson and Dr. M.M. Pervaiz of Spectral Sciences, Inc., Burlington, Massachusetts.

This report is a contribution to the Smart Weapons Operability Enhancement (SWOE) Program. SWOE is a coordinated, Army, Navy, Marine Corps, Air Force and DARPA program initiated to enhance performance of future smart weapon systems through an integrated process of applying knowledge of the broadest possible range of battlefield conditions.

Performance of smart weapons can vary widely, depending on the environment in which the systems operate. Temporal and spatial dynamics significantly impact weapon performance. Testing of developmental weapon systems has been limited to a few selected combinations of targets and environment conditions, primarily because of the high costs of full-scale field tests and limited access to the areas or events for which performance data are required.

Performance predictions are needed for a broad range of background environmental conditions and targets. Meeting this need takes advantage of significant DoD investments by Army, Navy, Marine Corps and Air Force in 1) basic and applied environmental research, data collection, analysis, modeling and rendering capabilities, 2) extensive target measurement capabilities and geometry models, and 3) currently available computational capabilities. The SWOE program takes advantage of these DoD investments to produce an integrated process.

SWOE is developing, validating, and demonstrating the capability of this integrated process to handle complex target and background environment interactions for a world-wide range of battlefield conditions. SWOE is providing the DoD smart weapons and autonomous target recognition (ATR) communities with a validated capability to integrate measurement, information base, modeling and scene rendering techniques for complex environments. The result of a DoD-wide partnership, this effort works in concert with both advanced weapon system developers and major weapon system test and evaluation programs.

The SWOE program started in FY89 under Balanced Technology Initiative (BTI) sponsorship. Present sponsorship is by the U.S. Army Corps of Engineers (lead service), the individual services, and the Joint Test and Evaluation (JT&E) program of the Office of the Director of Defense Research and Engineering (DDR&E), Office of the Secretary of Defense (OSD).

The Program Director is Dr. L.E. Link, Technical Director of the U.S. Army, Cold Regions Research and Engineering Laboratory (CRREL). The Program Manager is Dr. J.P. Welsh, CRREL. The Integration Manager is Mr. Richard Palmer, CRREL. The task areas and their managers are as follows: Modeling Task Area, LTC George G. Koenig, USAF, Geophysics Laboratory (GL), of the Air Force Phillips Laboratories; Information Bases Task Area, Mr. Harold W. West, PE, U.S. Army Engineer, Waterways Experiment Station (WES); Scene Rendering Task Area, Mr. Mike Hardaway, Corps of Engineers, Topographic Engineering Center (TEC); Validation Task Area, Dr. Jon Martin, Atmospheric Sciences Laboratory (ASL) of the Army Materiel Command.

TABLE OF CONTENTS

LIST OF ILLUSTRATIONS

LIST OF ILLUSTRATIONS (CONTINUED)

LIST OF TABLES

1. INTRODUCTION

In support of new systems for the detection and recognition of surface targets, the Smart Weapons Operability Enhancement (SWOE) Program has undertaken development of models to predict the infrared (IR) radiation from complex natural backgrounds. The SWOE program combines experimental data with modeling and simulation efforts, in order to fully consider the effects of natural environments during systems development.[1,2] This requires background models to simulate scenes with full 3-D effects at a nominal spatial resolution of about one meter. As part of this effort, energy budget models that predict an object's surface temperature will have to take into account the energy transport from the surfaces of various topographical features (vegetation, trees, soil, rocks, water, cultivated fields, roads, buildings, etc.) in both the visible and IR spectral regions. The simulation models must describe the major radiometric elements for scene generation, including thermal emission, atmospheric effects, and reflection of sun, earth and sky radiation.

An intermediate goal is the description of IR radiation from either a single tree or copse that would be found at the edge of a road or field at moderate northern latitudes. This report addresses one aspect of this problem, modeling the radiometric properties of leaves and bark. Surface Optics Corporation (SOC) measured the surface properties of bark and leaf samples from two trees.[3] Their data include the directional reflectance (DR) over 0.3 to 25 μm and the bidirectional reflectance (BRDF) at three wavelengths.

This report presents an analysis on these reflectance data, including reflectance models which are suitable for scene simulation models. A singular value decomposition (SVD) technique is used to justify a basic model assumption, factorization of the spectral and angular dependences into separate product functions. Details of the SVD technique are presented in Appendix A. An empirical reflectance model, previously developed by Spectral Sciences, Inc. (SSI), is applied to these data. The SOC data[3] are discussed in Section 2, while the directional and bidirectional reflectance models are briefly described in Section 3 with more details appearing in Appendix B. Some model parameters are listed in Appendix C.

2. OVERVIEW OF MEASUREMENTS

Surface optical properties of bark and leaf samples, taken from a single big-leaf aspen tree located in Maine, were measured by SOC. Leaves were also taken from an aspen tree in Lexington, Massachusetts. This overview is essentially taken from the SOC report;[3] the reader is directed there for more information, including a tabulation of the data. The total hemispherical directional reflectance (DR) was measured from 0.3 to 25 μm, and the bidirectional reflectance (BRDF) at three IR wavelengths. Since the leaves are translucent at shorter wavelengths, transmittance measurements were also made, but only for normal incidence ($\theta_i = 0$).

The DR is defined as the ratio of the total energy reflected to the incident source energy from the direction (θ_i,ϕ_i), where θ_i represents the incident beam zenith angle with respect to the local surface normal and ϕ_i is the incident azimuthal angle. The BRDF is the radiance reflected into a unit solid angle in the direction (θ_r,ϕ_r) divided by the total radiance incident in the direction (θ_i,ϕ_i). The angular directions are conveniently referenced to a spherical polar coordinate system (θ,ϕ), where θ represents the polar angle and ϕ the azimuthal angle. For the bark samples, 0° azimuth corresponds to the vertical direction of the bark as it existed on the tree. For the leaf samples, this direction was chosen to lie along the main vein running through them.

2.1 Bark Samples

Two bark samples were taken from the trunk of a Maine aspen tree at heights of 51 and 55 inches. Their properties are summarized in Table 1. For both the two bark and fifteen leaf samples, the dependence of the DR on sample orientation or azimuthal angle was found to be negligible. The only exception was FS4833 (bark sample No. 1), which is shown in Fig. 1 for an incident polar angle of 20° and perpendicular azimuthal angles. The FS numbers are assigned by SOC for sample identification. Minor differences occur in the 0.7 to 1.8 μm region with a maximum difference of 5.5% at about 1.3 μm. We consider these differences to fall well within expected limits of experimental uncertainties, possible statistical spread associated with bark from other similar trees and the accuracy of the reflectance model. It is appropriate to note that sample 1 did not appear very homogeneous due to the presence of surface fungi. Additional measurements on bark samples with moss buildup may be required before one can attribute DR differences to

Table 1. Properties of Bark Samples.

Format Number	Brief Sample Description	Sample Properties
FS4833	Bark Sample 1	Spotty appearance
	Time: 2:00 pm	Fungi growth
	Date: Sep 12, 90	DR dependent on orientation
	Orientation: West side	
	Height: 55 inch	
FS4834	Bark Sample 2	Homogeneous appearance
	Time: 2:16 pm	No moss growth
	Date: Sep 12, 90	DR independent of ϕ_i
	Orientation: North-east	
	Height: 51 inch	

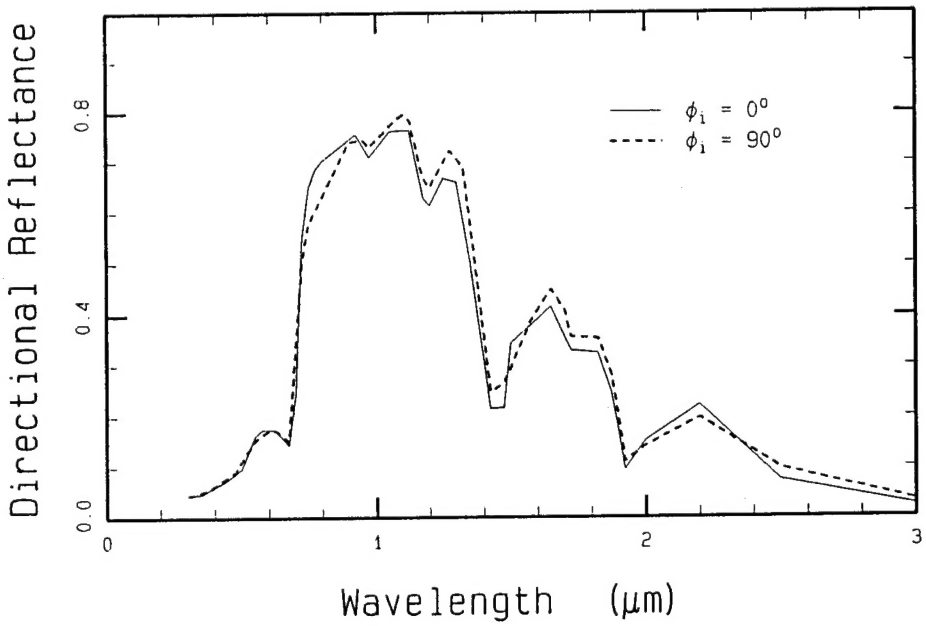

Figure 1. Spectral Variation of the DR for an Incident Polar Angle $\theta_i = 20^\circ$ and Two Azimuthal Directions $\phi_i = 0, 90^\circ$ for Bark Sample FS4833.

bark anisotropy. Since the effect of orientation of the bark sample is less than about 5%, azimuthal dependence is neglected in the model, and the bark samples are regarded as isotropic even in the presence of fungi.

2.2 Leaf Samples

Twenty leaf samples were taken from the Maine aspen tree from five small branches with multiple leaves. The branches were cut on September 12, 1990 at about 2:00 pm and shipped overnight to SOC. They were placed in bud vases so the leaves had an uninterrupted supply of water. Upon arrival, they were refrigerated until measured. The various measurements spanned a period of about two weeks. A second set of leaves from a different aspen tree in Lexington, MA, was obtained and shipped on October 19, 1990. These leaves were much drier and on the verge of turning color.

Illustrative leaf reflectance data are shown in Fig. 2, and a summary of these leaf samples is given in Table 2. Because of heat generated by the internal light sources in the instruments, the leaves dried significantly during measurement. Measurements were repeated on samples that had been left out to dry for several days, in order to study the effect of leaf moisture. Reflectances from both the top and bottom sides were measured. Full directional (for various θ_i values) and bidirectional reflectances were measured for the Maine samples, whereas the DR for $\theta_i=20^o$, and total transmission for $\theta_i=0^o$ were measured for the second batch of leaves.

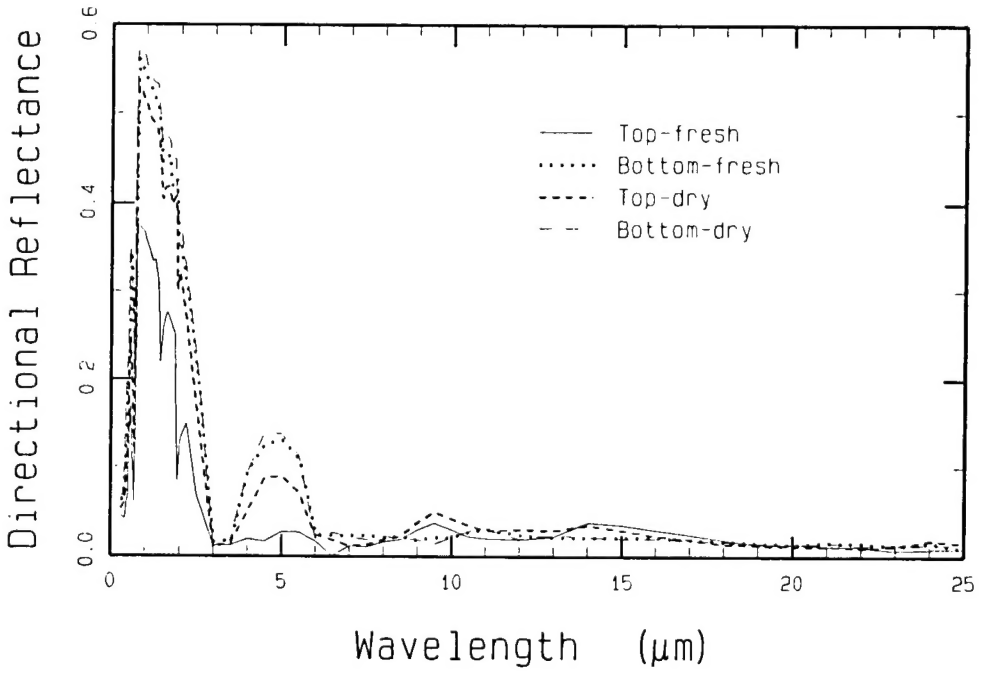

Figure 2. Spectral Variation of the DR at an Incident Polar Angle of $\theta_i=20^o$ for (Dry, Fresh) and (Top, Bottom) of Leaves From Samples FS4866 and FS4867.

Table 2. Properties of Leaf Samples.

Format Number	Brief Sample Description	Sample Properties
FS4835	Leaf Sample 1 Top Side Date: Sep 12, 90	Sample remained moist for wavelengths up to 1.6 μm for initial measurements DR dependent on moisture Both dry and moist data Full DR and BRDF data set
FS4836	Leaf Sample 2 Bottom Side Date: Sep 12, 90	Sample remained moist for for initial measurements DR independent of moisture Behavior similar to top-dry Both dry and moist data Full DR and BRDF data set
FS4866 to FS4881	8 Leaf Samples Top and Bottom Sides Date: Oct 19, 90	DR measured for ϕ_i=0,θ_i=20° Both dry and moist data
FS4882 to FS4885	4 Leaf Samples Date: Oct 19, 90	Scattered transmission at ϕ_i=0,θ_i=0°

No significant dependence on ϕ_i was observed for the directional reflectance on the leaves. Significant changes were observed between the top and bottom sides of the leaves and between the dry versus moist leaves. The changes due to the drying of the leaves were not as pronounced for the bottom side as they were for the top side. The moist sample actually began to dry during the measurements for wavelengths above 1.6 μm. The mismatch of the DR data from the two instruments at 1.6 μm indicates measurement uncertainties up to about 12% around this wavelength. Due to drying, the reflectance was constantly changing during the measurement process. The effect of this drying on the top side of the leaf was most noticeable in the near IR. When moist, the reflectance for the top side of the leaf is fairly flat from 3 to 25 μm, averaging about 3%. After drying, the reflectance for the top side shows a rise starting at 3.5 μm and ending at 6 μm with a peak value of about 8 to 10% at about 4.5 to 5 μm. This peak was also observed on the bottom side of the leaf, whether it was fresh or dry. From 0.5 to 2 μm, the reflectance from the top dry side is about 8 to 12% greater than the reflectance from the top fresh side. A

higher reflectance in the visible and near IR wavelengths is also seen in the data from the bottom side, whether fresh or dry. Figure 2 presents typical data from the Lexington, MA samples at $\theta_i=20^o$ which illustrate these trends. The main conclusion drawn from this figure (and other SOC data) is that the reflectance for the top side of the dry leaves resembles that of the fresh or dry bottom side. Hence only the first two data sets shown in Table 2 (FS4835 and FS4836) are needed to characterize the optical properties of these leaves. The samples chosen have a full set of DR and BRDF measurements.

For the sixteen leaves from Lexington, the DR was measured over the full 0.3 to 25 μm region for 20° incident angle. Four additional leaves from this batch were used to measure transmission in the same wavelength region. Transmission was also measured for the Maine samples FS4835 and FS4836.

Figure 3 shows the total transmission from the top and bottom side of a Maine aspen leaf (FS4835-36) and a Massachusetts leaf (FS4882). There is little difference between the top and bottom sides of the Maine leaf. However, there are some differences between the two leaves, some of which can be attributed to the leaves from Massachusetts being more dry and on the verge of turning color. Maximum differences (of the order of 15%) occur around 1 μm. Beyond 3 μm any differences are negligible.

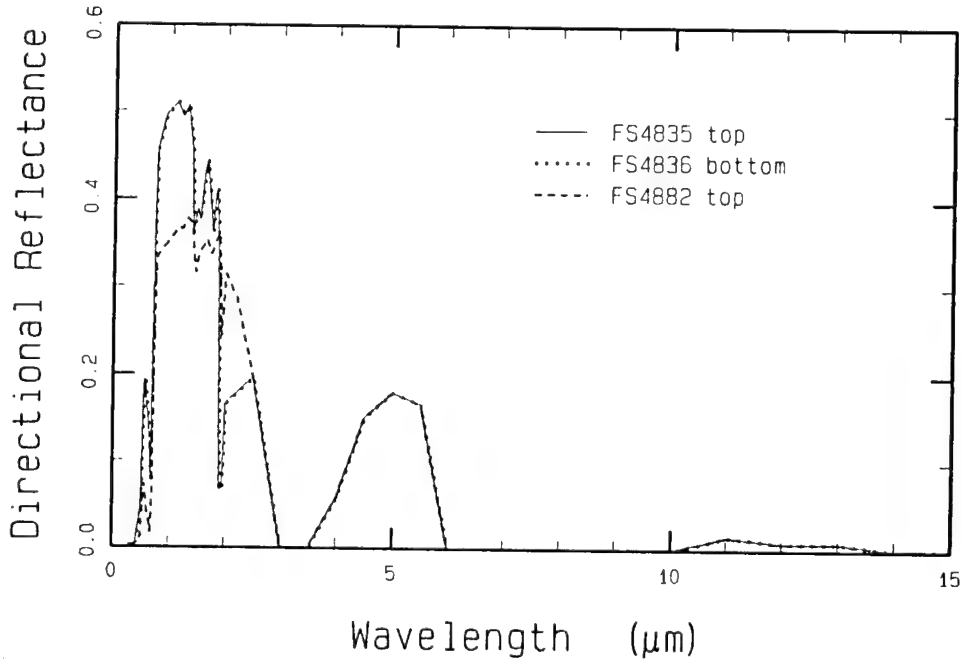

Figure 3. Spectral Transmittance at Normal Incidence for Maine (FS4835 and FS4836) and Massachusetts (FS4882) Leaves.

3. OVERVIEW OF ANALYSIS MODELS

This section provides an overview of the models used in the analysis. Additional details are given Appendices A and B. Appendix C lists a few values as a function of wavelength, for a typical set of bark and leaf samples, which may be useful as input parameters for the models. A key element in the modeling approach is the assumption that the total reflectance (directional or bidirectional) can be factored into a product of separate spectral and angular functions.

3.1 SVD Technique

The *Singular Value Decomposition* technique or *SVD* is a useful approach that allows one to separate a given data set into distinct contributions. It can diagnose that a given set of data can be written into a *variable separable* form. Separating the spectral and angular parts of reflectance and emittance functions allows the wavelength and angular dependencies to be integrated separately. For example, one may be interested in computing the total directional reflectance $\rho_T(\theta_i,\phi_i)$ of a surface for a given filter bandpass. This quantity is a weighted integral of the spectral directional reflectance $\rho(\theta_i,\phi_i,\lambda)$ over all wavelengths λ, with the weights being the filter spectral response function. The integration process is greatly simplified if one can factor the angular and spectral contributions of $\rho(\theta_i,\phi_i,\lambda)$. Another example is the total solar absorptance[3] which involves the weighted integration of absorptivity with the weights being the solar irradiance.

In this application, the SVD approach assumes a set of observations of a quantity a as a function of the discrete variables λ_i and θ_j with the following functional form

$$a_{ij} = a(\lambda_i,\theta_j) \quad , \tag{1}$$

where the element numbers i and j can be regarded as corresponding to the rows and columns of the measurement matrix $\{a_{ij}\}$. This quantity can be a matrix of directional reflectances, or any other quantity that is a function of two distinct variables. SVD separates the wavelength and angular parts, yielding the following form for the factorized product function

$$\hat{a}_{ij} = w_1 u_1(\lambda_i) v_1(\theta_j) \qquad (2)$$

as the leading term in a series expansion. Here $u_1(\lambda_i)$ and $v_1(\theta_j)$ are vectors that respectively signify the spectral and angular dependence of the variation. The quantity w_1 is a constant and is known as the first (or largest) singular value.

The predicted form of Eq. (2) may be regarded as a reasonable approximation (known as a rank 1 approximation) to Eq. (1) only if the magnitude of the dominant singular value w_1 is much larger than the next highest singular value in the series. This is a necessary condition, but it is generally not sufficient to justify factorization into two distinct contributions. The rank 1 approximation is justified when its normalized root-mean-square (rms) errors, relative to the maximum value in the data set, are small. This condition suffices to justify the premise of factorization.

3.2 Reflectance Model

A factorizable bi-directional reflectance model developed by Spectral Sciences, Inc. (SSI) describes the emission and reflection of radiation from surfaces. This empirical model provides a reasonable representation of reflectance data while being suitable for incorporation into large modeling codes. The model attempts to economically characterize the reflectance associated with paint surfaces. Using it for the bark and leaf samples would be calculationally convenient and would ease the work needed for additional coding. The parameters applicable to vegetative samples and other surfaces could be added as part of a data base accessed by the overall simulation software. Two key features of the model are a semi-empirical formulation for the angular dependence of diffuse scatter and emission, and a finite width to the angular distribution for specular scatter. The width of the specular lobe is based on a model for surface roughness developed by Trowbridge and Reitz.[4] The reader is referred to Appendix B for more information. The model is briefly described here to provide a continuity with the data analysis and to illustrate its factorization properties.

Since the radiation incident on a surface can be either absorbed, transmitted, or reflected, the DR can be written as

$$\rho(\theta_i,\phi_i,\lambda) = 1 - \epsilon(\theta_i,\phi_i,\lambda) - \tau(\theta_i,\phi_i,\lambda) \quad , \qquad (3)$$

where ϵ is the emissivity and τ is the transmissivity of the surface. To model the DR, we assume surface isotropy which implies that the dependence on orientation or azimuthal angle can be ignored. If one further assumes that their spectral and angular dependences can be factorized, then the emissivity and transmissivity are given by

$$\epsilon(\theta_i,\lambda) = \epsilon_\lambda \, g(\theta_i) \tag{4}$$

and

$$\tau(\theta_i,\lambda) = \tau_\lambda \, p(\theta_i) \quad . \tag{5}$$

For the bark samples τ_λ is zero; for the leaves, the measured transmissivity is negligible beyond 5 μm. Applying the SVD analysis to 1-ρ for these cases leads to the determination of the functions ϵ_λ and $g(\theta_i)$. The observed functional form for $g(\theta_i)$ is consistent with the following empirical function (See Appendix B)

$$g(\theta_i) = \frac{1}{1 + b^2 \tan^n \theta_i} \quad , \tag{6}$$

where b is an adjustable parameter and is referred to as grazing angle reflectivity. A value n = 1 gives acceptable agreement with the DR data. Note that $g(\theta_i) = 1$ at normal incidence so the normalization function G(b) defined by Eq. (B-8) in Appendix B is not included in ϵ_λ. The normalization function for the angular distribution requires the spectral part ϵ_λ to be associated with total hemispherical emittance of the surface element. The exponent n for the tangent function is 2 in the SSI reflectance model described in Appendix B. The angular dependence of the transmittance may be similar to Eq. (6).

The reflected radiation is divided into its specular and diffuse components. Thus the BRDF is given by

$$f_r = f_r(\theta_i,\phi_i;\theta_r,\phi_r) = f_s + f_d \quad , \tag{7}$$

where the subscripts d and s denote the diffuse and specular parts, respectively. This is also assumed for the total hemispherical radiation, i.e.,

$$\rho(\theta_i,\lambda) = \rho_d(\theta_i,\lambda) + \rho_s(\theta_i,\lambda) \quad . \tag{8}$$

The total diffuse reflectance is assumed to have the same functional form for the spectral and angular parts as the emissivity, i.e.,

$$\rho_d(\theta_i,\lambda) = \rho_{d\lambda}\, g(\theta_i) \quad , \tag{9}$$

with ($g(\theta_i)$ given by Eq. (6). The diffuse BRDF is independent of the azimuthal angles and is given by

$$f_d(\theta_i,\phi_i;\theta_r,\phi_r) = f_d(\theta_i;\theta_r) = \frac{1}{\pi}\, g(\theta_r)\, \rho_{d\lambda}\, g(\theta_i) \quad . \tag{10}$$

A modified form of a model developed by Trowbridge and Reitz[4] is used to describe specular reflection. This is given by

$$f_s(\theta_i,\phi_i;\theta_r,\phi_r) = \frac{1}{4\pi}\, \rho_s(\lambda,\theta_i)\, \frac{h(\alpha)}{H(\theta_i)}\, \frac{1}{\cos\theta_r} \quad , \tag{11}$$

where α is the glint angle, i.e., it is the angle between the surface normal and the bisector for the incident (θ_i,ϕ_i) and reflected (θ_r,ϕ_r) directions. The azimuthal dependence in the BRDF is contained in the angle α. The function $h(\alpha)$ is given by

$$h(\alpha) = \left[\frac{1}{e^2\cos^2\alpha + \sin^2\alpha}\right]^2 \quad , \tag{12}$$

where the eccentricity parameter e describes the angular width of the specular lobe. The function $H(\theta)$ is a normalization integral that normalizes the reflectance over all observer angles to the total specular reflectance; its functional form is given by

$$H(\theta) = \frac{1}{2e^2}\left[(1-e^2)\mathrm{Cos}\theta + \{2e^2+(1-e^2)\mathrm{Cos}^2\theta\}/\sqrt{(1-e^2)^2\mathrm{Cos}^2\theta+4e^2}\right] \quad . \tag{13}$$

Here θ refers to θ_i. Writing the expressions $g(\theta_i)$ and $g(\theta_r)$ as g_i and g_r, respectively, and writing the functions $h(\alpha)$ and $H(\theta_i)$ without their arguments, the full expression for the BRDF from Eqs. (7-11) becomes

$$f_r(\theta_i,\phi_i;\theta_r,\phi_r) = \frac{1}{\pi}\, g_r\, \rho_{d\lambda}\, g_i + \frac{h}{4\pi H\cos\theta_r}\left[1 - g_i(\epsilon_\lambda+\rho_{d\lambda}) - \tau_\lambda\, p(\theta_i)\right] \quad . \tag{14}$$

The parameters b, ϵ_λ and τ_λ are determined from the DR data. Furthermore, the angular function for the transmittance $p(\theta_i)$ is either zero for opaque surfaces or is determined from the transmittance measurements by the procedure discussed in the next section. The remaining parameters in this expression are $\rho_{d\lambda}$ and e, a surface roughness parameter

which enters the above expression through Eq. (12). These two parameters are determined via a non-linear least squares fit to the BRDF data.

3.3 Two-Stream Diffusion Model

In order to gain a rough estimate for the transmissivity as a function of polar angle θ_i, a two-stream diffusion model[5] developed for cloud scattering (a collection of independent scatterers) was considered. These models predict the total radiation field as the sum of four basic elements: (1) thermal emittance, (2) transmitted radiation, (3) backscattered radiation, and (4) scattered solar radiation. Most two-stream models utilize three parameters:

(1) ω, albedo,
(2) a_f, asymmetry factor, and
(3) ℓ, optical depth.

The albedo ω is the fraction of the extinguished incident radiation that is lost due to scattering. Physically, it represents the probability that, for a given photon/particle interaction, the photon will be scattered as opposed to absorbed. Smaller values for the scattering albedo imply most of the radiation is lost to absorption. An albedo of unity corresponds to a surface which can only scatter and not absorb.

The asymmetry factor a_f is the mean value of the cosine of the scattering angle. For isotropic scattering, $a_f = 0.0$; for highly forward scattering, it approaches 1, and it tends to -1 when backward scattering predominates. From the emissivity values for an optically thick medium, one can make reasonable choices for ω and a_f. For the calculations shown here, we considered the measurements at $\lambda = 1$ μm and chose the values $\omega = 0.98$, and $a_f = 0.4$.

The observed transmittances were then used to estimate a reasonable value for the optical depth. For the 1 μm data of the sample, an optical depth of about 4.0 is obtained. Figure 4 shows the resulting angular variation of the transmittance for three different optical depths. This variation in the transmittance is approximately linear between 20 and 80°, which is not incompatible with our analysis of the leaf data.

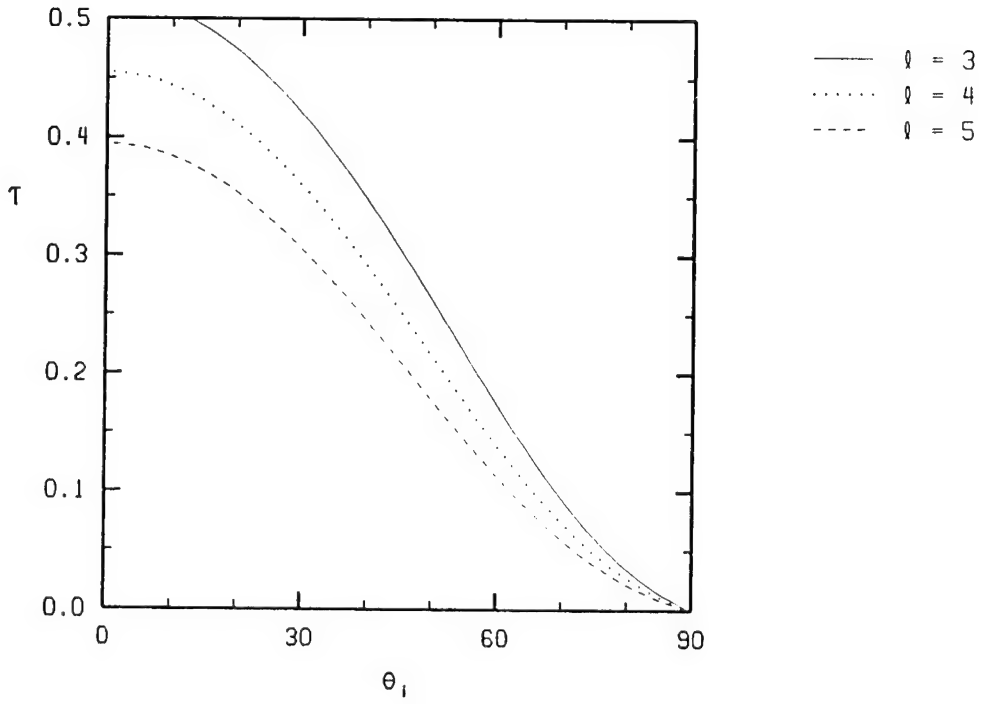

Figure 4. Angular Variation of the Transmittance for Three Values of the Optical Depth ℓ. The Albedo $\omega = 0.98$, and the Asymmetry Factor $a_f = 0.4$

4. DATA ANALYSIS

All the bark and leaf measurements were considered in analyzing the SOC reflectance data. This discussion focuses on four data sets, two bark (FS4833 and FS4834) and two leaf (FS4835 and FS4836), because they have a more complete set of measurements (i.e., various incident angles and for dry/moist conditions). The analysis of the DR data starts with the SVD approach to smooth the data and to demonstrate their factorability. This is followed by application of the reflectance model. A simple model for leaf transmittance is presented to help describe the DR in the visible and near IR spectral regions and to take advantage of the transmittance measurements. The BRDF data have little angular structure (i.e., the surfaces are very diffuse), so we focused on just the DR measurements.

In applying the SVD approach to the DR data, the directional emissivity, $\epsilon = 1 - \rho$, is separated into two distinct components, spectral and angular. Including the second order term in the SVD expansion yields a somewhat better fit, especially at shorter wavelengths. The second order terms from the SVD analysis for the leaves were identified with the transmissivity at these wavelengths.

4.1 Bark Samples

The SVD decomposition was applied to the directional emissivity matrix $\epsilon(\theta_i,\lambda)$ for the two bark samples. The emissivity matrix is defined by Eq. (3) with τ_λ=0.0 and includes the measured DR at angles θ_i = (20, 30, 40, 50, 60, 70, 75, 80°) and 45 wavelengths over 0.3-25 μm. For subsequent discussions, the subscript for θ_i is dropped. Table 3 summarizes the SVD results. The first singular values w_1 are substantially larger than the second ones w_2. The rank 1 approximation provides an adequate description of the data, especially for $\lambda \geq 3.0$ μm, since its rms errors are less than 10%. In other words, the factorization assumption used by the reflectance model is reasonable. The maximum deviation for both samples occurs between 1 and 3 μm. Figure 5 shows the variation of $e_1(\lambda)$ with wavelength. For the one-component SVD model $e_1(\lambda)$ equals ϵ_λ, the bark emissivity. The upper figure shows the full 0.3-25 μm spectral region, and the lower one shows 0.3-3.0 μm on an expanded scale. The lower figure also shows the spectral dependence of the second (smaller) component of the SVD expansion. Overall this term is small, but it does become significant around 1.5 μm, which is near the

Table 3. Summary of SVD Analysis for Bark Samples.

Sample	Band(μm)	w_1	w_2	e^1_{rms}	e^2_{rms}
FS4833	.3 - 25	13.99	.40	.03	.01
	.3 - 3.	9.66	.37	.03	.01
	3. - 25.	10.47	.16	.07	.02
FS4834	.3 - 25	14.82	.25	.02	.01
	.3 - 3.	10.72	.22	.02	.01
	3. - 25.	10.59	.10	.01	.01

w_1 largest singular value for SVD
w_2 second largest singular value for SVD
e_{rms} relative rms error for ranks 1 & 2

minimum of the first term. The second terms were required to be ≥ 0, so that they could be given a physical interpretation and identified with a model component.

The two component SVD model can be converted into a two component emissivity/transmissivity model by finding positive components which can reproduce the SVD results. This is obtained by forming linear functions of the SVD components to obtain positive but non-orthogonal vectors.

$$E_1(\lambda) = \bar{u}_1(\lambda) + c\,\bar{u}_2(\lambda) \tag{15a}$$

$$E_2(\lambda) = d\,\bar{u}_1(\lambda) - \bar{u}_2(\lambda) \quad , \tag{15b}$$

and

$$g_1(\theta) = \bar{v}_1(\theta) + d\,\bar{v}_2(\theta) \tag{16a}$$

$$g_2(\theta) = c\,\bar{v}_1(\theta) - \bar{v}_2(\theta) \quad , \tag{16b}$$

where the top bar means $\bar{u} = u_n\sqrt{W_n}$ and $\bar{v} = v_n\sqrt{W_n}$. The coefficients c and d are arbitrary. We consider a range where all components are positive. For the barks, c and d were chosen so that the first components would most closely follow the spectral data. Thus values of (c,d) of (0.37,0.21) and (0.28,0.16) were selected for barks FS4833 and FS4834,

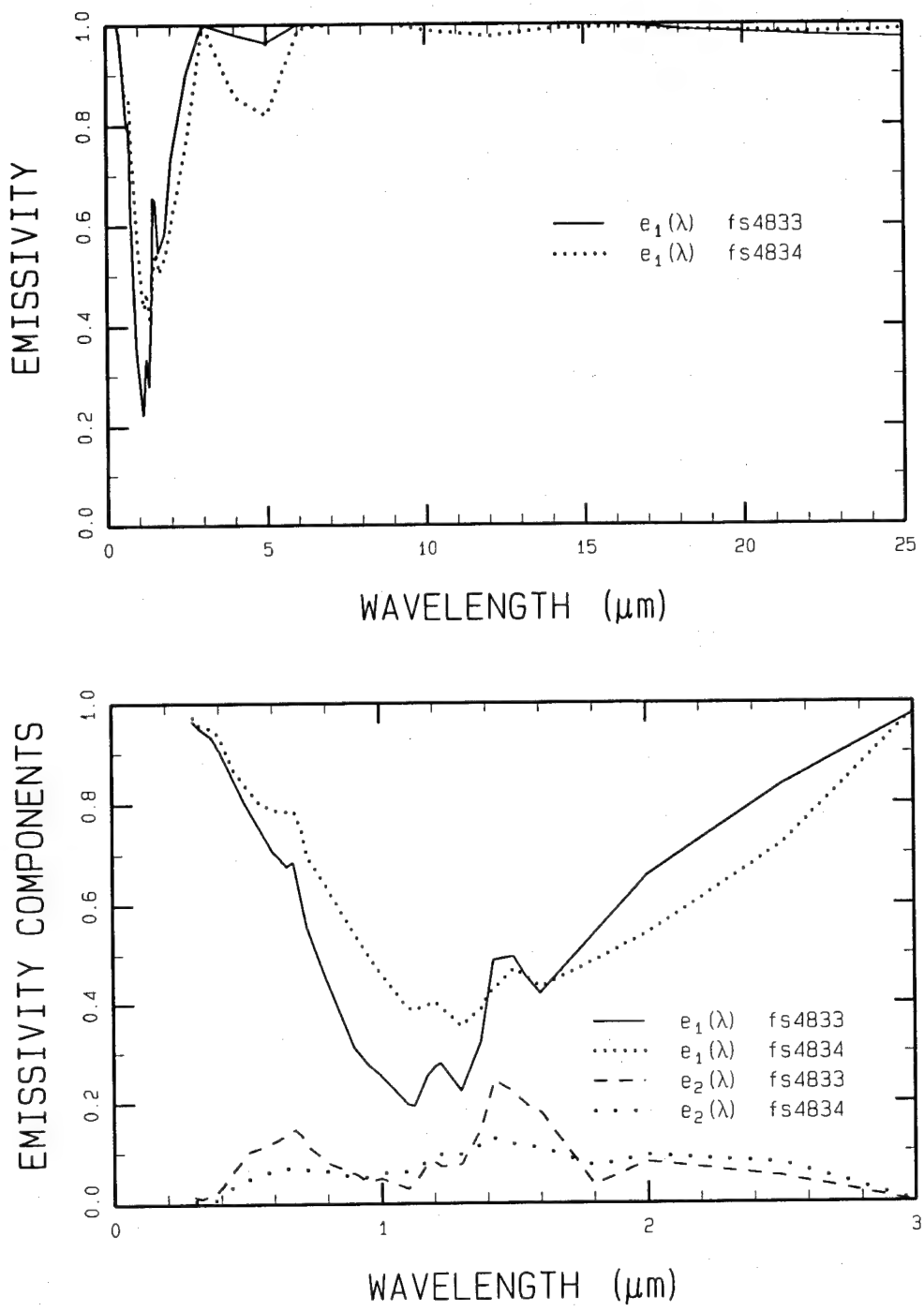

Figure 5. Spectral Distribution Functions for the Bark Samples Resulting From the SVD Analysis. a) The Full 0.3-25 μm Spectral Region, and b) the 0.3-3.0 μm Region.

respectively. Figure 5b shows the resultant relative contributions of the two spectral emissivity components in the 0.5-3.0 spectral region. (At longer wavelengths the $e_2(\lambda)$ contributions are very small.) The selection for the leaf samples, discussed below in Subsection 4.2, was based on identification of $e_2(\lambda)$ with the leaf transmissivity.

The angular functions from the data and the resulting SVD values for one of the bark samples are shown in Fig. 6. The data, which are shown in Fig. 6a, include additional spectral measurements at 20°, resulting in the extra structure around 2.0 μm. The rank 1 and 2 SVD results are shown in Figs. 6b and 6c, respectively. Because it only appears at one angle, the extra spectral structure of the 20° measurements has been lost. If important to an application, these data points could be added to the spectral distribution function $e_1(\lambda)$.

Turning to the angular part of the data, a non-linear least-squares regression was applied to the $g_i(\theta)$ data from the SVD analysis. The model angular function $g(\theta)$ is defined by Eq. (6). The resultant values of the parameter b are given in Table 4, and comparisons to the angular parts of the SVD expansions are shown in Fig. 7. The functional form of Eq. (6) was applied to the angular functions for two values of the

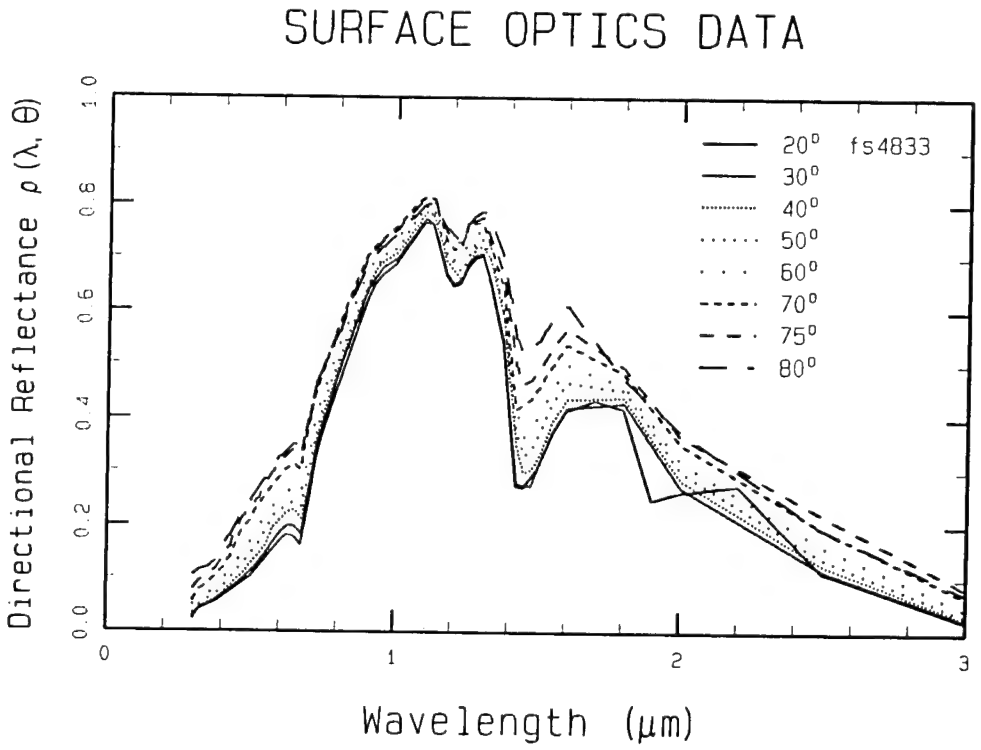

Figure 6a. SOC Data for Bark Sample FS4833.

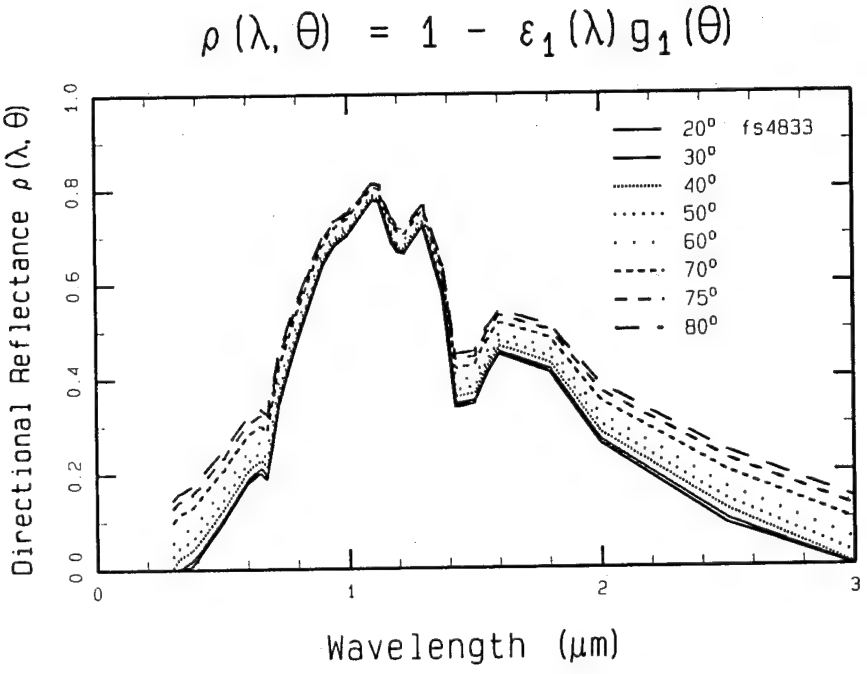

Figure 6b. Rank 1 Approximation From the SVD Expansion in 1-ρ.

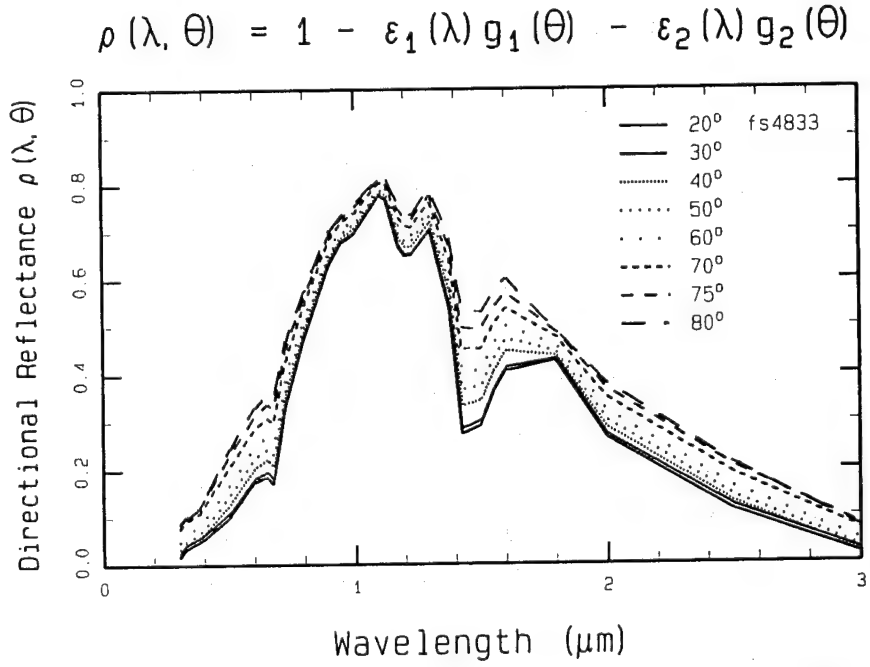

Figure 6c. Spectral and Angular Distributions Resulting From the Rank 2 SVD Expansion in 1-ρ.

Table 4. Least Squares Regression Parameters for $g(\theta)$.

Sample	b_1	n_1	b_2	n_2
FS4833	.20	1	.59	2
FS4834	.13	1	.50	2

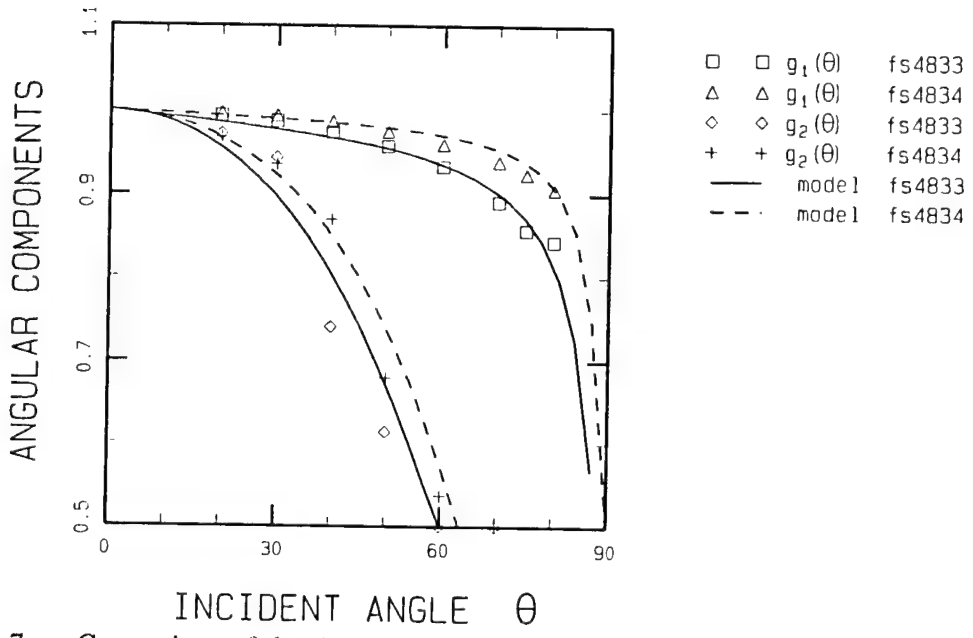

Figure 7. Comparison of the Angular Distribution Functions $g_i(\theta)$,i=1,2 and Fits Using Eq. (6) to Both the Rank 1 and 2 SVD Terms.

parameter n. We found slightly better agreement with the data using n=1 for the stronger component, and n=2 for the second component.

Illustrative comparisons of the full reflectance function, Eq. (3), to the SOC data are shown in Fig. 8. The angular dependence of the DR for three wavelengths, 1, 5, and 10 μm, are plotted in the figure for the second bark sample. The calculated curves only include the parameters determined for the first term in the SVD expansion. These fits generally agree well with the data, though the agreement with the data around 1.0 μm would be improved by modeling both terms in the SVD expansion.

Better agreement could also be achieved if one allowed the parameter b to be a slowly varying function of wavelength (and uses a least squares fit to determine this

wavelength dependence). However, we feel that these fits with constant b are adequate for present applications, and additional computational complexity is not needed. Alternately, the approach described above, which uses parameters obtained from applying the SVD approach in narrower spectral regions and including the next higher terms, could be used to develop a matrix of values for the parameters b and n. This would be the next step in upgrading the model.

4.2 Leaf Samples

The SVD analysis for the leaf directional emissivity shows the factorability of the angular and spectral dependencies. Each of the two leaf data sets, FS4835 and FS4836, was processed three times: the full data set, long wavelengths where the leaves are essentially opaque ($\lambda \geq 3\ \mu m$), and shorter wavelengths where they are translucent ($0.3 \leq \lambda \leq 3.\ \mu m$). The results are summarized in Table 5. Again the second singular values, w_2, are much smaller than the first ones. The rms error for both the first and second order expansions are quite small. Since spectral transmittance measurements were made and the leaves are significantly translucent in the near IR, the second term is identified with the leaf transmittance.

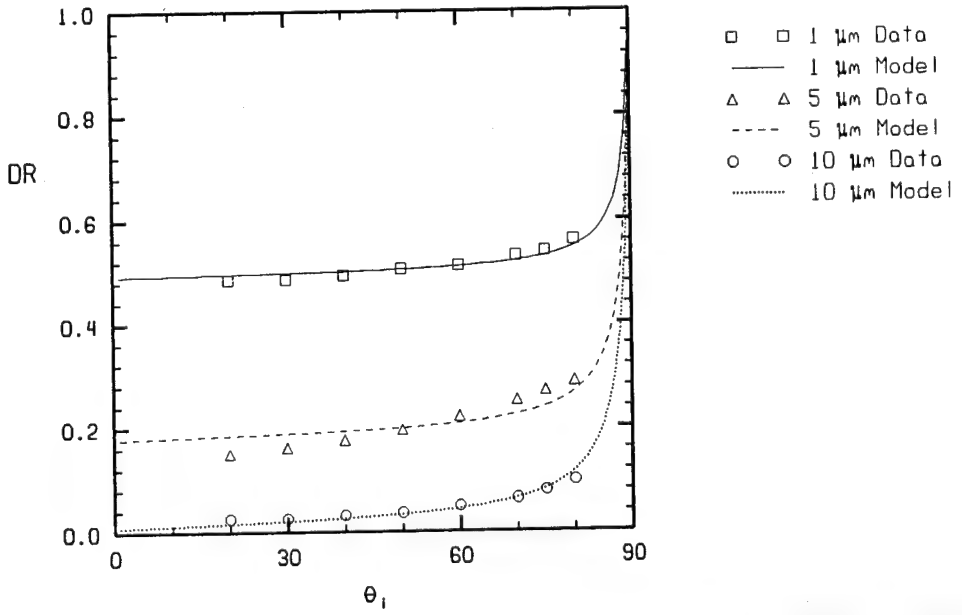

Figure 8. Comparison of the SOC Directional Reflectance Data With Model Predictions to Bark Sample 2, FS4834.

Table 5. SVD Decomposition for Leaves.

Sample	Band(μm)	w_1	w_2	e^1_{rms}	e^2_{rms}
FS4835	.3 - 25	14.76	.33	.03	.01
	.3 - 3.	10.64	.31	.04	.01
	3. - 25.	10.58	.05	.03	.02
FS4836	.3 - 25	14.05	.53	.05	.01
	.3 - 3.	9.76	.44	.04	.01
	3. - 25.	10.58	.05	.03	.01

Plots of the spectral emissivity for the two data sets are shown in Fig. 9. Figure 9a presents the full spectral region, 0.3-25. μm, and Figs. 9b and 9c show the emissivity and transmissivity, respectively, in the 1-3 μm region. For the latter two figures, the vectors from the SVD analysis were rotated according to Eqs. (15) and (16) in order to obtain components which could be identified with the leaf emissivity and transmissivity. The parameter d was minimized so the angular term $g_1(\theta)$ would match its long-wavelength value as closely as possible. The parameter c was selected so that the $e_1(\lambda)$ would resemble an estimated ϵ_λ at 0° incident angle. Numerical values for (c,d) are (1.68,0.19) and (1.38,0.24) for samples FS4835 and FS4836, respectively. The ϵ_λ at 0° identified as data was obtained by extrapolation of the values of 1-ρ at 20 and 30° to 0° and subtracting τ_λ from the result. Comparisons of the two model components with the emissivities and transmittances are shown in Figs. 9b and 9c. The agreement here is quite good, and much better agreement of the combined two component model with the directional reflectance data is obtained in this spectral region (0.3-3.0 μm). These results suggest that quite acceptable predictions for the transmissivity as a function of zenith angle could be extracted from the directional reflectance data.

The spectral and angular distribution of the SOC data for the first leaf sample are shown in Fig. 10a. Only the short wavelength data are shown because the results for e^1_{rms} shown in Table 5 indicate that the data are well fit by a single SVD term at longer wavelengths. Figures 10b and 10c show the data sets resulting from the first and second order applications of SVD, respectively. As can best be seen around 1.7 μm, the second order SVD agrees with the data better the first order. These smoothed data bases are then used to generate parameters for the reflectance model.

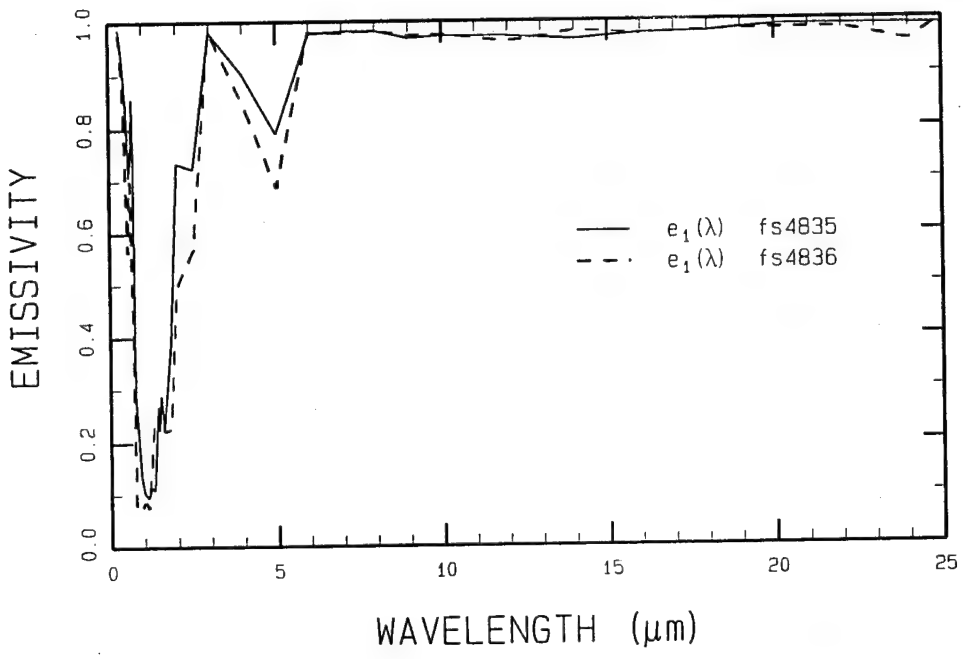

Figure 9a. Spectral Emissivity for the Top and Bottom Leaf Samples Resulting From the SVD Analysis.

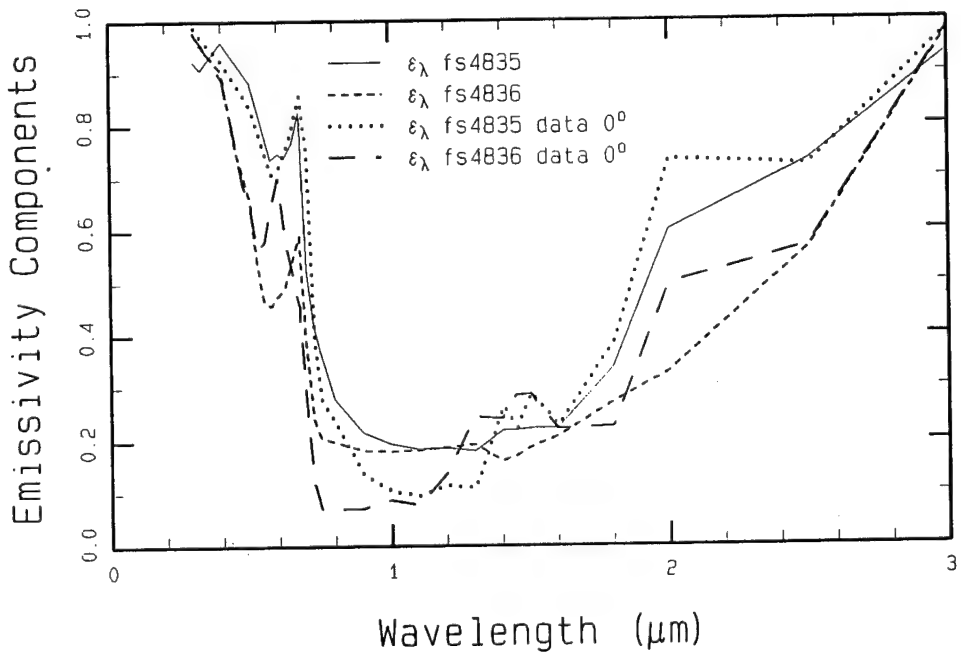

Figure 9b. Estimated Emissivity Components at 0° Incidence.

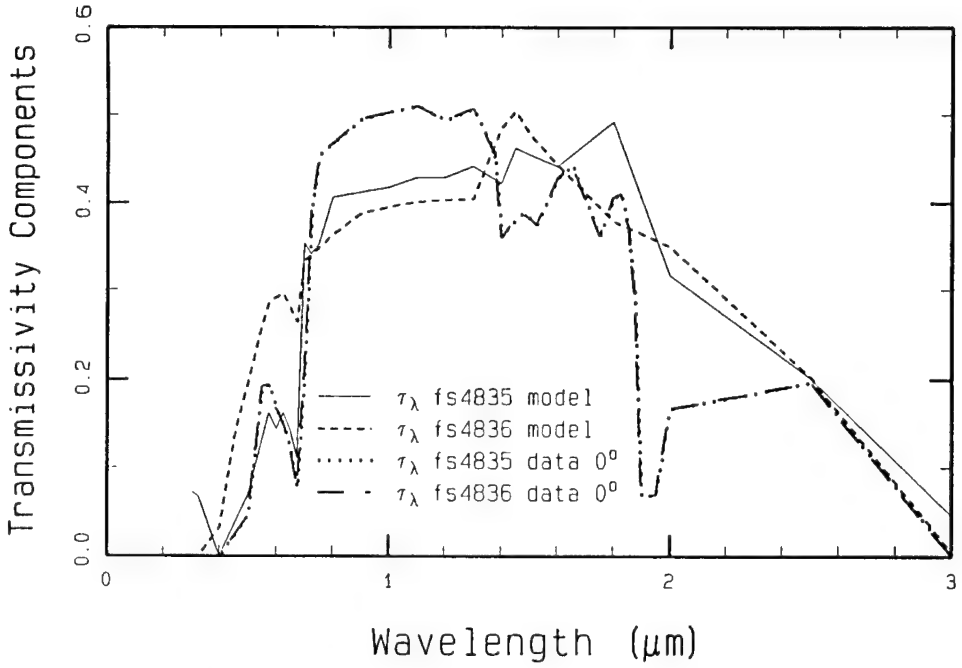

Figure 9c. Transmissivity Components at 0° Incidence.

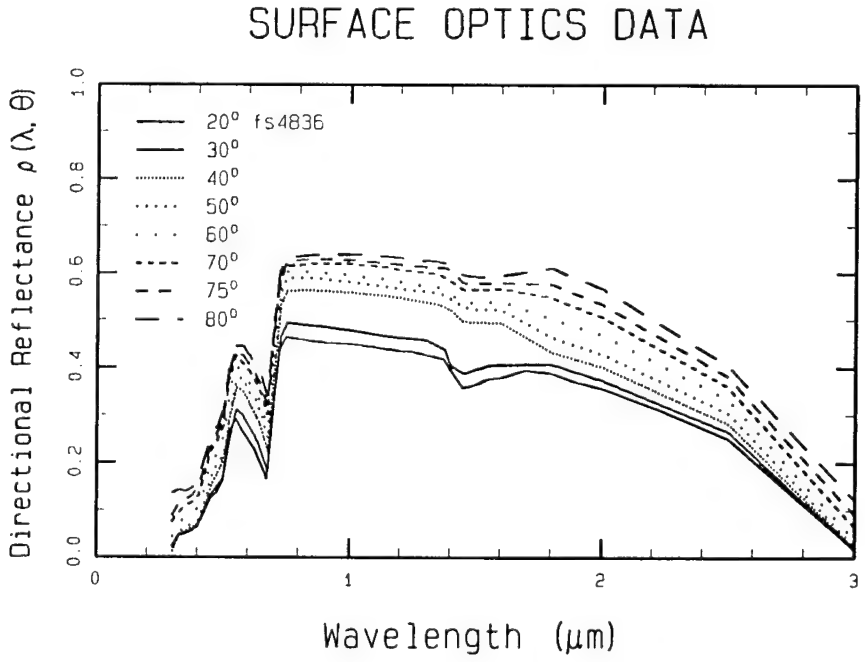

Figure 10a. SOC Data for Leaf Sample FS4836.

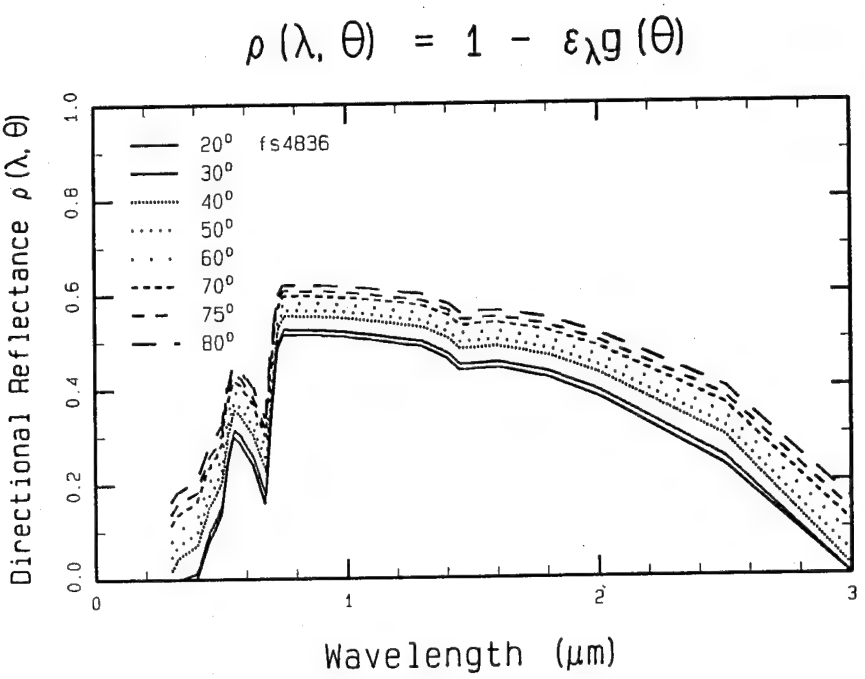

Figure 10b. Approximation From the SVD Rank 1 Expansion of 1-ρ.

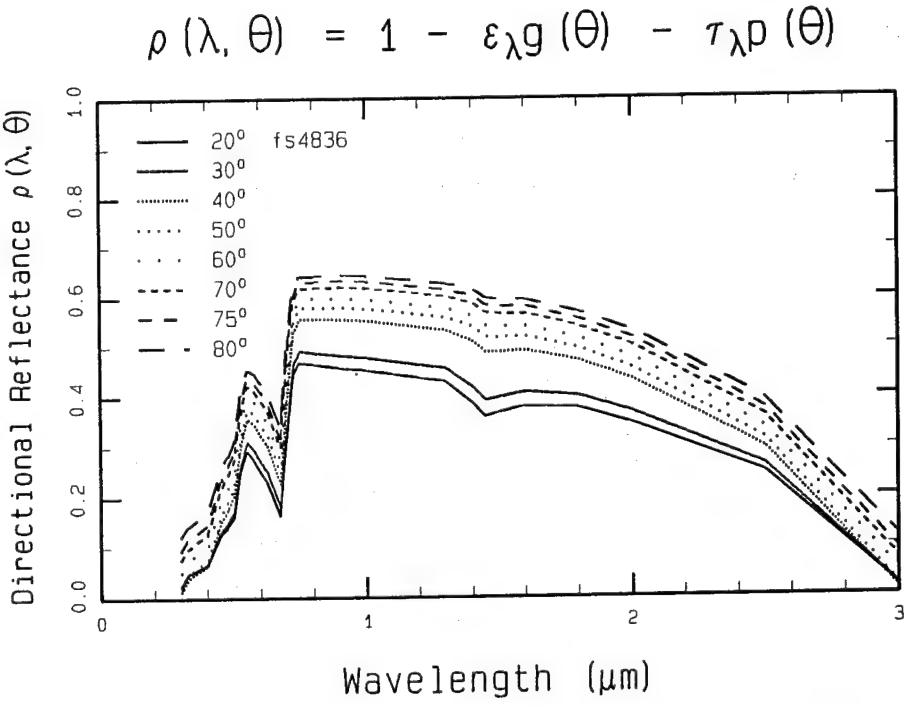

Figure 10c. Spectral and Angular Distributions From the Rank 2 SVD Expansion of 1-ρ.

Figure 11 shows the scaled angular dependences of $g_i(\theta)$ for $\lambda > 6$ μm. The symbols correspond to the data $g_1(\theta)$ obtained from the rank 1 SVD analysis. The lines correspond to the model $g(\theta_i)$ of Eq. (5) with n = 1. The angular functional forms for these wavelengths are nearly identical for the top and bottom sides, so any differences in the reflectance can be attributed to the spectral function τ_λ. Recommended model parameters for the leaves are given in Table 6.

Figure 12 presents illustrative comparisons of the functional form of Eq. (3) to the DR measurements for the top leaf sample (FS4835) at wavelengths of 1, 5 and 10 μm. There is fairly good agreement with the measured data.

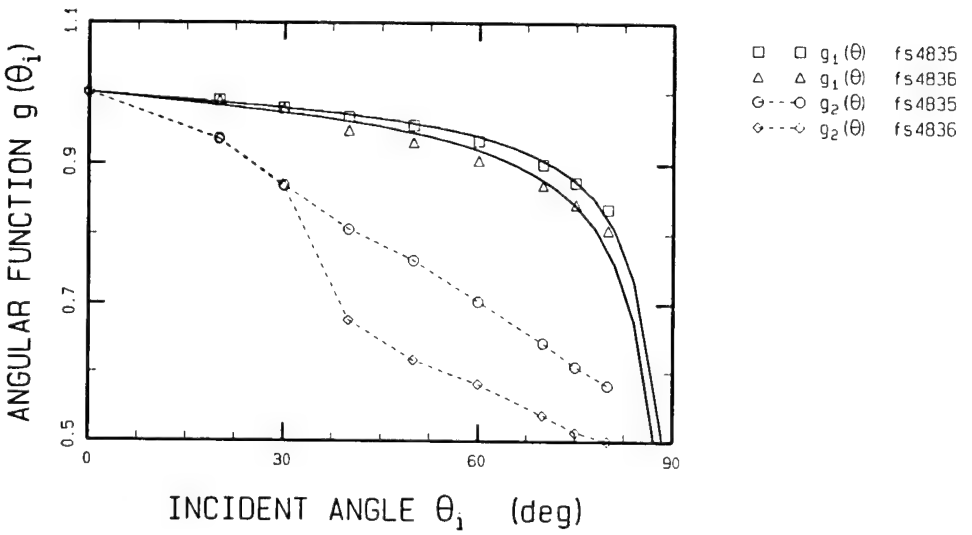

Figure 11. Angular Distribution Functions $g(\theta)$ From the SVD and Model Fits Using Eq. (6).

Table 6. Fit Parameters for $g(\theta)$.

Sample	b_1	n_1
FS4835	.19	1
FS4836	.22	1

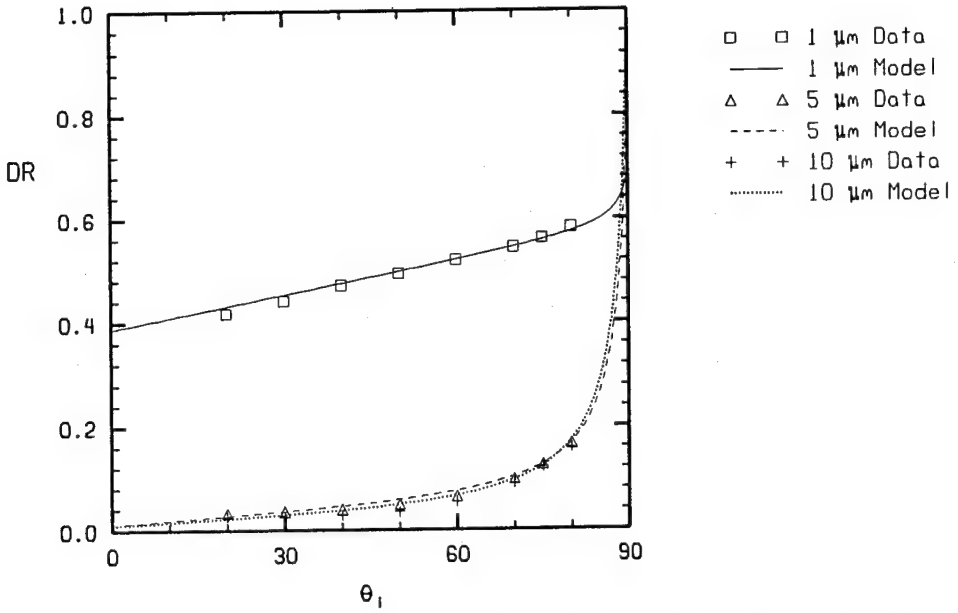

Figure 12. Comparison of the Angular Dependence of the DR Data With Model Predictions for Leaf Sample 1 (FS4835).

5. CONCLUSIONS AND RECOMMENDATIONS

5.1 Summary

The first conclusion to be drawn from these data is that the vegetative samples exhibit IR reflectance and emittance properties which are significantly different from the visible spectral region. We have introduced an empirical reflectance-emittance model which describes the essential spectral and angular features seen in the data. In applications to scene generation with computer models, the equations for the directional emissivity

$$\epsilon(\lambda,\theta) = \frac{\epsilon_\lambda}{1 + b \tan\theta} \tag{17}$$

and for the directional reflectance

$$\rho(\theta_i, \lambda) = 1 - \frac{\epsilon_\lambda}{1 + b \tan\theta_i} - \tau_\lambda (1 - a\theta_i) \quad . \tag{18}$$

provide acceptable fits to the data. These equations are suitable for integration into larger calculational models. (In fact, similar equations have been used to describe the properties of aircraft surface coatings.) From Fig. 11, a reasonable value for the parameter a is $1/90^o$.

For the bark and leaf samples discussed here, the dependence of the DR on orientation or azimuthal angle was found to be negligible. One bark sample with significant surface fungi showed differences up to 5% in the near IR when it was rotated by 90^o. The average difference was less than 4% in the range between 0.3 and 1.8 μm, and no significant differences due to orientation were observed at longer wavelengths. Therefore orientation effects were neglected in the proposed reflectance models. As discussed in the SOC report,[3] no significant dependence on ϕ_i was observed for the directional reflectance of the leaves.

Some spectral and angular differences were observed between the top and bottom sides of the leaves and between dry and moist leaves. The changes due to drying were not as pronounced for the bottom side of the leaf as they were for the top side. The effect of drying was most noticeable around 1.0 μm. One conclusion from these data is that the reflectance for the top side of the dry leaves resembles that of the bottom side. A single

reflectance model, with the same parameters, may be considered adequate to characterize the DR and BRDF variations associated with the top-dry, bottom-fresh and bottom-dry samples. Different parameters may be needed for the top-fresh leaves.

Little difference between the top and bottom sides of the leaves were evident in the transmission data. Only normal transmission measurements were made. Significant differences between the transmission measurements in the visible and near IR region of [0.3,5] μm were seen for leaves from different sources (possibly different leaf thicknesses) and with different moisture content. All leaves (whether dry or fresh) were essentially opaque beyond 5 μm.

The SVD data clearly indicated that the directional emissivity can be factored into distinct specular and angular contributions. The SSI reflectance model described in Appendix B is adequate for the bark and leaf samples, especially when the $\tan\theta$ factor is linear instead of quadratic. A linear term is added to the leaf model to provide an acceptable engineering approximation for the transmittance. Additional measurements at non-normal incident angles are needed to extend this linear assumption to a more physically reasonable formulation for the angular contribution.

5.2 Recommendations

Additional transmittance measurements are needed for incident polar angles other than 0°. Such measurements will clearly identify the functional dependence of transmittance on the incident polar angle. These measurements should also be repeated for moist versus dry conditions so that the effect associated with the moisture content can be quantified. The leaf transmittance must also be correlated with observed thickness of the leaves at the time of the measurements.

It is absolutely vital to consider leaf and bark samples from other sources found in typical vegetative environments. These measurements are essential to completion of a data base for various sources to support a comprehensive scene generation model. In addition, samples should also be collected at different times of the year to quantify seasonal effects. It may also be possible to lump together similar vegetative samples when plant physiology is taken into account. For example, leaf surfaces in hot and arid climates are typically thick and lustrous to avoid the loss of moisture during prolonged dry periods. It may be possible to lump together the samples from such similar environments. In any case, additional measurements and studies are needed before such specific inferences can be made.

Additional modeling will be required once the appropriate measurements have been carried out. These may include the determination of the model parameters for various samples at various times of the year. In addition, a more elaborate volumetric transmission model may be needed, once the effects associated with transmission are better measured. The compiled data base of various vegetative and other background environments should be integrated into a comprehensive simulation software package. With the advent of powerful, massively parallel super computers, it may be possible to routinely run high resolution scenes and simulations. The data bases being developed for SWOE must be ready to address this requirement.

6. REFERENCES

1. J. A. Conant, L. S. Dean, B. P. Sandford, and G. J. Koenig, "BTI-Smart Weapons Operability Enhancement (SWOE) Modeling Overview," IRIS Speciality Group on Targets, Backgrounds, and Discrimination (January 1990).

2. J. A. Conant, L. S. Dean, B. P. Sandford, and G. J. Koenig, "Improvements in Background Scene Generation Capabilities in Coordination with the BTI SWOE Program," IRIS Speciality Group on Targets, Backgrounds, and Discrimination (January 1990).

3. J. T. Neu, R. S. Dummer, M. Beecroft, P. McKenna, and D. C. Robertson, "Surface Optical Property Measurements on Bark and Leaf Samples," Phillips Laboratory Rpt. PL-TR-91-2009 (December 1990) ADA240714.

4. T. S. Trowbridge and K. P. Reitz, "Average Irregularity of a Rough Surface for Ray Reflection," J. Opt. Soc. Am., 65, 531 (1975).

5. S. Chandrasekhar, Radiative Transfer (Dover Publications, Inc., New York, 1950).

APPENDIX A: SVD TECHNIQUE

A very powerful technique which can be used to justify separating a given data set into two distinct contributions is *Singular Value Decomposition* or *SVD*. This technique can precisely diagnose that a given set of data can be written into a *variable separable* form. SVD methods are based on a theorem of linear algebra that states that any r x c matrix A whose number of rows r is greater than or equal to its number of columns c, can be approximated as a product of an r x p column-orthogonal matrix U, a p x p diagonal matrix W with positive elements, and the transpose of a c x p row-orthogonal matrix V. Here p is the rank of the original matrix A. Also note that $p \leq c \leq r$ and that approximation becomes exact when $p = c$, i.e., all the variations in the original matrix A can be explained by a rank c decomposition.[A1] The shapes of various matrices can be made clear by

$$A_{rxc} \approx U_{rxp}\, W_{pxp}\, V^{T}_{pxc} \qquad p \leq r \leq c \tag{A-1}$$

and the exact decomposition[A2] is

$$A_{rxc} = U_{rxc}\, W_{cxc}\, V^{T}_{cxc} \qquad r \leq c \ . \tag{A-2}$$

The diagonal form of W implies its elements satisfy the conditions

$$w_{ij} = \begin{cases} 0\,, \text{ when } i \neq j \\ \\ w_i \geq 0\,, \text{ when } i = j \end{cases} \qquad 1 \leq i,j \leq c \tag{A-3}$$

The matrices U and V are each orthogonal in the sense that their columns are orthonormal,

$$\sum_{i=1}^{r} u_{ij}\, u_{ik} = \delta_{jk} \qquad 1 \leq j,k \leq c \ , \tag{A-4}$$

$$\sum_{i=1}^{c} v_{ij}\, v_{ik} = \delta_{jk} \qquad 1 \leq j,k \leq c \ . \tag{A-5}$$

The elements for the exact rank c SVD, from Eq. 2, can be shown to be

$$a_{ij} = \sum_{k=1}^{c} u_{ik} w_k v_{kj} \quad . \tag{A-6}$$

If the matrix W is singular with only the first p ($p \leq c$) non-zero elements, then the decomposition can be expressed exactly by a rank p SVD, i.e.,

$$a_{ij} = \sum_{k=1}^{p} u_{ik} w_k v_{kj} , \quad p \leq c , \quad w_k = 0 \text{ for } p \leq k \leq c \quad . \tag{A-7}$$

In particular, if w_1 is the largest eigenvalue and if it is substantially more than other diagonal elements, then using just the first term and hence the rank 1 SVD approximation are justified. A variable separable form

$$a_{ij} \approx u_{i1} w_1 v_{1j} , \quad 1 \leq i \leq r , \quad 1 \leq j \leq c \tag{A-8}$$

is justified. Here $U = \{u_{i1}\}$ represents a column vector with r elements and $V^T = \{v_{1j}\}$ represents a row vector with c columns. Thus if the observed or measured matrix has the elements

$$a_{ij} = a(\lambda_i, \theta_j) , \quad 1 \leq i \leq r , \quad 1 \leq j \leq c \tag{A-9}$$

as a function of discrete wavelengths λ_i and discrete angular values θ_j, then a rank 1 approximation states that wavelength and angular parts can be separated out as

$$\hat{a}_{ij} = w_1 u(\lambda_i) v(\theta_j) , \quad 1 \leq i \leq r , \quad 1 \leq j \leq c \tag{A-10}$$

where the carat ($\hat{}$) indicates the predicted values and the SVD analysis yields the singular value w_1 and the vectors $u(\lambda_i)$ and $v(\theta_j)$. The discrete form can be converted to a continuous function with variables λ and θ by defining interpolating functions, with the resultant $\hat{a}$ being written as

$$\hat{a}(\lambda,\theta) = w\, u(\lambda)\, v(\theta) \quad . \tag{A-11}$$

The rank 1 (or higher rank) approximation can be justified if the normalized root-mean-square (rms) errors due to this approximation can be shown to be small compared to unity. The rms errors are given by

$$e = \frac{1}{(rc - 1)\, a_m} \sum_{i=1}^{r} \sum_{j=1}^{c} \left(a_{ij} - \hat{a}_j \right)^2 , \qquad \text{(A-12)}$$

where the maximum matrix element a_m is given by

$$a_m = \max (a_{ij}) , \quad 1 \leq i \leq r , \quad 1 \leq j \leq c . \qquad \text{(A-13)}$$

The SVD analysis is applied to the directional reflectance data for the bark and leaf samples. When these samples are opaque, this technique verifies that the directional emissivity, $\epsilon = 1\text{-}\rho_d$, can be separated into two distinct spectral and angular components. Additional analysis is needed to determine the angular and spectral components associated with transmissivity. In principle, one can recursively apply the SVD analysis to determine the contributions due to additional effects. Thus after determining the functional forms of spectral and angular contributions of ϵ from the opaque regions, one can apply the SVD analysis to $1\text{-}\rho_d\text{-}\epsilon$ on the translucent regions and factor out the spectral and angular contributions associated with transmittance.

REFERENCES

A1. W. H. Press, B. P. Flannery, S. A. Teukolsky, and W. T. Vetterling, *Numerical Recipes*, Cambridge University Press (1986).

A2. G. Strang, *Linear Algebra and its Applications*, Academic Press (1980).

APPENDIX B: BI-DIRECTIONAL REFLECTANCE MODEL

A bi-directional reflectance model was developed by SSI to describe the emission and reflection of radiation from surfaces. Although this discussion is based on opaque planar surfaces, the model can be extended to transmitting surfaces. Two key features of the model are a semi-empirical formulation for the angular dependence of diffuse scatter and emission, and a finite width to the angular distribution for specular scatter. The width of the specular lobe is based on a model for surface roughness developed by Trowbridge and Reitz.[B1]

The SSI model is empirical in that its emittance and reflectance parameters are derived from analysis of reflectance data. Surface reflectance results from many underlying physical parameters and processes; examples are the dielectric properties of the scattering surface (expressed as the complex index of refraction), surface roughness effects, subsurface (or volume) scattering, thickness of a paint layer, scattering from a substrate, and polarization effects.[B1-B5] In addition one has to consider the combined effects of aging and weather for surfaces used on aircraft or other operational vehicles. The object of this model is to arrive at a simplified parameterization of a paint's reflectance properties that is suitable for incorporation into a code for calculating target signatures. This includes scattered sunshine, earthshine, and skyshine plus surface emissions.

Before proceeding, a nomenclature list for the various quantities used in reflectance modeling is presented. The list is based on published definitions which should be used in order to standardize the nomenclature.[B6,B7] For an exhaustive discussion of this issue, the reader is directed to Reference (B7). The quantities used here are given in Table B.1. General properties used for reflectance modeling are described in Subsection B.1, followed by the formulation of the semi-empirical model in Subsection B.2.

B.1 General Reflectance Properties

B.1.1 Spectral Reflectance

The reflectance model is built around four parameters: the diffuse reflectance (ρ_d), the emittance (ϵ), and two parameters (b and e) which describe the directional and bi-directional reflectance. We make the physically reasonable assumption that b and e vary

Table B.1. Nomenclature List for the Various Quantities used in Reflectance Modeling.

SYMBOL	DEFINITION	UNITS
$\rho,\rho(\lambda)$	(spectral) surface reflectance	-
$\rho(\lambda,\theta)$	directional spectral reflectance	-
$\epsilon,\epsilon(\lambda)$	(spectral) surface emittance	-
$\epsilon(\lambda,\theta)$	direction spectral emittance	-
$\alpha,\alpha(\lambda)$	(spectral) surface absorptivity	-
α	angle between glint vector and surface normal	rad.
A	area	m^2
E	irradiance (replaces H)	W/m^2
$f_r, f_r(\theta_i,\phi_i;\theta_r,\phi_r)$	BRDF Bi-directional reflectance distribution function	sr^{-1}
f_d, f_s	diffuse, specular part of the spectral BRDF	-
f_{rI}	BRIDF Bi-directional reflected intensity distribution function	sr^{-1}
I	source radiant intensity (replaces J)	W/sr
L	radiance (replaces N)	$W/m^2/sr$

slowly with wavelength, so that they can be treated as constant over finite wavelength regions. For the BRDF and related quantities,

$$f_r(\theta_i,\phi_i;\theta_r,\phi_r;\lambda) = f_r(\theta_i,\phi_i;\theta_r,\phi_r)\,\rho(\lambda) = f_r\,\rho(\lambda) \qquad \text{(B-1)}$$

where f_r (the BRDF) gives the angular dependence of the reflected radiation. We assume factorization so that the spectral and angular properties are independent of each other.

B.1.2 Radiation Laws

Conservation of energy requires that radiation incident on a surface be either absorbed, transmitted or reflected. This requires that

$$\alpha + \tau + \rho = 1 \tag{B-2}$$

where α, τ, ρ are the absorptivity, transmittance, and reflectance. This is also true for the spectral quantities. Excepting transparent surfaces like aircraft canopies, surfaces are opaque, and $\tau(\lambda) = 0$. Thus,

$$\alpha(\lambda) + \rho(\lambda) = 1 \tag{B-3}$$

Note that Eqs. (B-2) and (B-3) are not always valid for each of the polarization components.[B7] Kirchoff's law states that the absorptivity and emissivity of a blackbody in thermal equilibrium are equal.[B3] This is valid totally and spectrally,[B7] i.e.,

$$\alpha = \epsilon \quad \text{and} \quad \alpha(\lambda) = \epsilon(\lambda) \tag{B-4}$$

This assumption is used to relate the absorption of incident radiation at angles (θ_i,ϕ_i) to the surface directional emissivity.

B.1.3 Viewing Geometry

Consider a planar surface element of area A. Its orientation in space is specified by the polar angles (θ,ϕ) of its normal; θ is measured from the zenith, and ϕ is measured from the x-axis. The coordinate axes are illustrated in Fig. B1. The same coordinate system is used to specify the direction to the observer (θ_r,ϕ_r) and to the sun (θ_i,ϕ_i). The unit vectors specifying the directions towards the observer and illumination source are $\hat{o}$ and $\hat{s}$, respectively. Thus, the directions of $\hat{o}$ and $\hat{s}$ are given by (θ_r,ϕ_r) and (θ_i,ϕ_i), respectively.

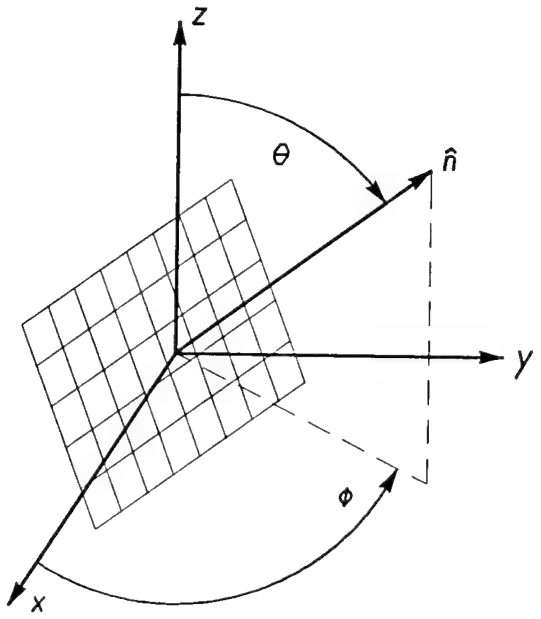

Figure B1. Coordinate Axes for a Surface Element.

B.2 Formulation of the Semi-Empirical Model

B.2.1 Model Assumptions

Various angles for defining the scattering geometry are shown in Fig. B2. For simplicity, the surface normal lies along the z-axis. The unit vectors $\hat{o}$ and $\hat{s}$ point towards the observer and source, respectively. The glint vector $\hat{g}$ is the unit vector for the bisector of the angle between $\hat{o}$ and $\hat{s}$. It is given by

$$\hat{g} = (\hat{o} + \hat{s})/\sqrt{2(1 + \hat{o} \cdot \hat{s})} \quad . \tag{B-5}$$

B.2.1.1 Factorization of Angular and Spectral Dependencies

The angular dependence of the emissivity and the reflectivity is partially independent of the wavelength.

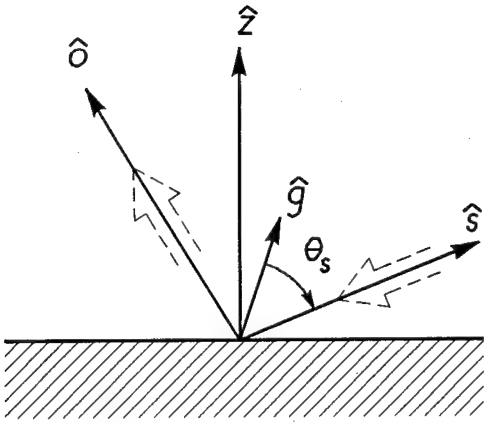

Figure B2. Angles and Directional Vectors for Scattering by a Surface Element.

B.2.1.2 Angular Dependence of Emissivity

The directional and spectral dependence of the emissivity is given by

$$\epsilon(\lambda,\theta) = \epsilon(\lambda)\,\frac{g(\theta)}{G(b)} \tag{B-6}$$

where

$$g(\theta) = \frac{1}{1 + b^2\tan^2\theta} \tag{B-7}$$

By requiring $\epsilon(\lambda)$ to be the total hemispherical emittance of the surface element, G(b), the normalization constant for the angular distribution, is given by

$$G(b) = \frac{1}{\pi}\int_0^{\pi/2}\sin\theta d\theta\int_0^{2\pi}d\phi\,\frac{\cos\theta}{1 + b^2\tan^2\theta}$$

$$= \frac{1}{1 - b^2}\left[1 - \frac{b^2}{1 - b^2}\log\,(1/b^2)\right] \quad . \tag{B-8}$$

The cosine factor gives the effective area of the surface element. The constant b is empirical and is determined from surface reflectance data. It takes the emissivity to zero as θ_r approaches 90°. A Lambertain surface emits equally in all directions and is given by $b = 0$.

B.2.1.3 Total Reflectance

Consider an incident, well collimated beam of light like that coming from the sun. From Eq. (B-4) the amount of energy in a wavelength interval absorbed by a surface equals the emissivity of the surface. The reflected radiation is divided into diffuse and specular components, so that

$$f_r(\theta_i,\phi_i;\overline{\pi/2},\overline{2\pi}) = \rho_s(\theta_i) + \rho_d(\theta_i)$$
$$= 1 - \epsilon(\lambda,\theta_i) \quad , \tag{B-9}$$

where the subscripts identify the specular and diffuse contributions and the bar indicates integration over all reflection directions (i.e., the total reflectance). Figure B3 shows the angular dependence of the total reflectance predicted by Eq. (B-9) for three illustrative values of b.

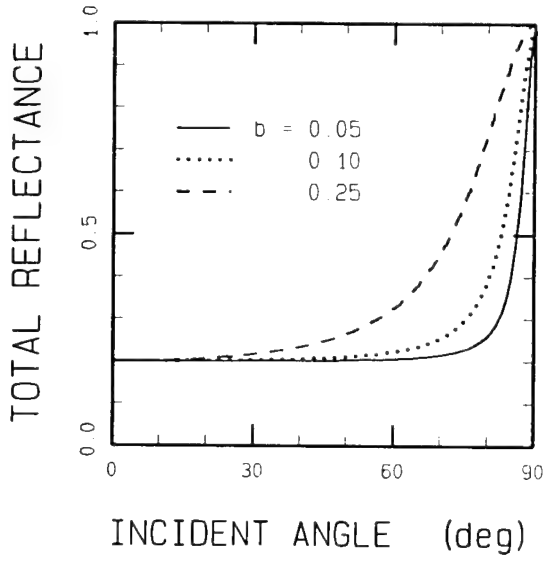

Figure B3. Angular Dependence of the Total Reflectance for Three Values of the Parameter b.

B.2.2 Diffuse Reflectance

Diffuse reflectance is assumed to be an average property of the surface resulting from subsurface scattering and from multiple scattering due to surface roughness on the microscopic level. The amount of radiation available for diffuse scattering varies with the angle of the incident beam. We assume that the directional dependence from an illuminated surface is the same as its emissivity. We then assume that the scattering process is symmetrical, e.g.,[B7]

$$f_r(\theta_i,\phi_i;\theta_r,\phi_r) = f_r(\theta_r,\phi_r;\theta_i,\phi_i) \quad , \tag{B-10}$$

and that the diffuse BRDF is given by

$$f_d(\theta_i,\phi_i;\theta_r,\phi_r) = \frac{1}{\pi} g(\theta_r)\rho_d(\lambda)g(\theta_i)/[G(b)]^2 \quad . \tag{B-11}$$

The amount of diffusely scattered energy is given by $\rho_d(\lambda)g(\theta_i)$, and the angular distribution of that radiation is given by $g(\theta_r)$. The diffusely scattered energy is given by

$$I_d(\theta_i,\theta_r) = \frac{1}{\pi} (E_{inc}\mathrm{Cos}\theta_i) f_d(\theta_i,\phi_i;\theta_r,\phi_r) \tag{B-12}$$

B.2.3 Specular Reflectance

A modified form of a model developed by Trowbridge and Reitz[B1] is used to calculate the specular reflection. They showed that the optical properties of a rough surface can be described by an equivalent circular ellipsoid with eccentricity e. In our model this parameter e describes the angular width of the specular lobe (i.e., the effect of surface roughness). The finite width of the angular distribution for spectral scattering is due to single scattering from this curved elliptical surface. A finite surface element is composed of many such micro-elliptical surfaces. The function $h(\alpha)$ is the surface structure function. The resulting BRDF is given by

$$f_s(\theta_i,\phi_i;\theta_r,\phi_r) = \frac{1}{4\pi}\rho_s(\lambda,\theta_i)\frac{h(\alpha)}{H(\theta_i)}\frac{1}{\cos\theta_r} \tag{B-13}$$

$$h(\alpha) = \frac{1}{[e^2\cos^2\alpha + \sin^2\alpha]^2} \qquad \text{(B-14)}$$

where α is the angle between the glint vector ($\hat{g}$) and surface normal, and $\cos\alpha = \hat{g} \cdot \hat{n}$.

Trowbridge and Reitz define $\rho_s(\lambda,\theta_s)$ as the Fresnel reflection coefficient for scattering at an angle θ_s for the refraction and absorption indices n and k of a dielectric surface. Here, the total specular reflection coefficient, $\rho_s(\lambda,\theta_i)$, is used for the angle θ_i as defined by

$$\rho_s(\lambda,\theta_i) = 1 - \rho_d(\lambda,\theta_i) - \epsilon(\lambda,\theta_i) \quad . \qquad \text{(B-15)}$$

Since $\rho_s(\theta_i)$ gives the fraction of the incident energy which undergoes specular reflection, it is required that the integral of Eq. (B-13) over all observer angles (θ_r,ϕ_r) be normalized to ρ_s. Thus,

$$H(\theta_i) = \frac{1}{4\pi}\int d\Omega_r h(\alpha) = \frac{1}{2e^2}\left[(1 - e^2)\cos\theta + [2e^2 + (1 - e^2)^2(\cos^2\theta)]/\sqrt{(1 - e^2)^2\cos^2\theta + 4e^2}\right] \qquad \text{(B-16)}$$

The energy scattered specularly for given incident and exciting directions is

$$I_s(\theta_i;\theta_r) = (E_{inc}\cos\theta_i)\, f_s(\theta_i,\phi_i;\theta_r,\phi_r)\, A \cos\theta_r$$

$$= (E_{inc}\cos\theta_i)\frac{\rho_s(\theta_i)}{4\pi}\frac{h(\alpha)}{H(\theta_i)} A \qquad \text{(B-17)}$$

Maximum specular scatter occurs when $\alpha = 0$.

An example of specular scattering for three different values of the parameter e is shown in Fig. B4. The BRDF is calculated for an angle of 20° for the incident radiation and for a total reflectivity (specular only) of 0.20.

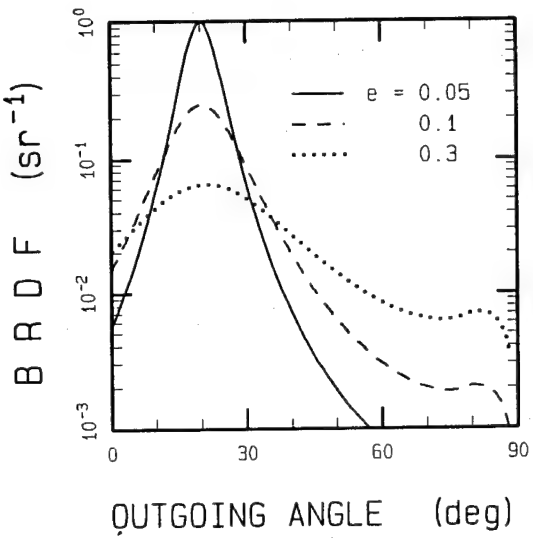

Figure B4. The BRDF for Incident Radiation at 20° and for Three Values of the Parameter e.

B.2.4 Shadowing and Obscuration

As the observer angle θ_r approaches 90°, the predicted amount of specularly reflected energy remains finite. This leads to divergences in the BRDF as θ approaches 90°. The data shown by Torrence and Sparrow exhibit this divergence, but with a sharp cut-off at 90° so that there is a peak in the BRDF around 85°. The divergence in the BRDF arises from the parameterization of the surface roughness as a single equivalent curved surface (ellipsoidal) that scatters for all angles. Shadowing and obscuration of scattering surface elements occur for grazing angles because the surface is planar in the macroscopic sense; this causes a cut-off at 90°. Convenient cut-off factors are

$$d(\theta) = \frac{1}{1 + \delta \, \mathrm{Tan}\theta} \quad , \tag{B-18}$$

and

$$d(\theta) = \frac{1}{1 + \delta^2 \, \mathrm{Tan}^2\theta} \quad , \tag{B-19}$$

Both factors lead to very messy normalization integrals when combined with the specular scattering function, Eq. (B-14). One way to get around this is to note that the cut-off is only significant in the 80-90° range and that Eq. (B-14) is approximately constant except for incident angles near 90°. Equation (B-19) is used in this model to cut-off the BRDF with δ = b and normalized to 1.0 at θ = 80°.

B.4 References

B1. T. S. Trowbridge and K. P. Reitz, "Average Irregularity of a Rough Surface for Ray Reflection," J. Opt. Soc. Am., 65, 531 (1975).

B2. F. E. Nicodemus, "Directional Reflectance and Emissivity of an Opaque Surface," Appl. Opt., 4, 767 (1965).

B3. K. E. Torrance and E. M. Sparrow, "Theory for off-Specular Reflection from Roughened Surfaces," J. Opt. Soc. Am., 57, 1105 (1967).

B4. J. T. Neu and R. S. Dummer, "Theoretical and Practical Implication of the Bidirectional Reflectance of Spacecraft Surfaces," AIAA Journal, 7, 484 (1969).

B5. J. C. Leader, "Analysis and Prediction of Laser Scattering from Rough-Surface Materials," J. Opt. Soc. Am., 69, 610 (1979).

B6. W. L. Wolfe and G. J. Zissis (Eds.), The Infrared Handbook, Office of Naval Research, Department of the Navy, Washington, DC (1978).

B7. F. E. Nicodemus, J. C. Richmond, J. J. Hsia, I. W. Ginsberg, and T. Limperis, "Geometrical Considerations and Nomenclature for Reflectance," NBS Monograph 160, National Bureau of Standards (1977).

APPENDIX C: TYPICAL NUMERICAL PARAMETERS

Tabulations of some numerical parameters for a typical bark (FS4834, with no moss) and leaf (FS4836, bottom-fresh) sample as a function of wavelength are given. These typical values can be used to compute the directional reflectance at other non-zero angles. The values of DR, emissivity, and transmissivity at zero incidence are provided here.

Bark Sample

$\lambda(\mu m)$	$\rho(0,\lambda)$	ϵ_λ
0.300	0.008	0.992
0.325	0.035	0.965
0.375	0.041	0.959
0.400	0.050	0.950
0.450	0.087	0.913
0.500	0.107	0.893
0.550	0.129	0.871
0.600	0.138	0.862
0.650	0.139	0.861
0.675	0.141	0.859
0.700	0.184	0.816
0.725	0.233	0.767
0.775	0.273	0.727
0.800	0.308	0.692
0.900	0.407	0.593
0.950	0.452	0.548
1.000	0.486	0.514
1.100	0.553	0.447
1.125	0.556	0.444
1.200	0.509	0.491
1.300	0.556	0.444
1.375	0.503	0.497
1.400	0.466	0.534
1.500	0.408	0.592
1.600	0.451	0.549
1.800	0.436	0.564
2.000	0.353	0.647
2.500	0.199	0.801
3.000	0.015	0.985

$\lambda(\mu m)$	$\rho(0,\lambda)$	ϵ_λ
4.000	0.120	0.880
5.000	0.138	0.862
6.000	0.022	0.978
7.000	0.015	0.985
8.000	0.013	0.987
9.000	0.015	0.985
10.000	0.026	0.974
12.000	0.035	0.965
14.000	0.018	0.982
16.000	0.024	0.976
18.000	0.027	0.973
20.000	0.023	0.977
22.000	0.047	0.953
24.000	0.025	0.975
25.000	0.035	0.965

Leaf Sample

$\lambda(\mu m)$	$\rho(0,\lambda)$	ϵ_λ	τ_λ
0.300	0.022	0.978	0.000
0.325	0.042	0.958	0.000
0.400	0.063	0.892	0.045
0.450	0.116	0.764	0.120
0.475	0.121	0.687	0.192
0.500	0.156	0.651	0.193
0.525	0.271	0.563	0.166
0.550	0.272	0.579	0.149
0.575	0.237	0.641	0.122
0.600	0.222	0.701	0.077
0.625	0.203	0.587	0.210
0.675	0.151	0.458	0.391
0.700	0.281	0.265	0.454
0.725	0.415	0.117	0.468
0.750	0.434	0.071	0.495
0.800	0.427	0.070	0.503
0.900	0.418	0.072	0.510
1.000	0.419	0.087	0.494
1.100	0.416	0.077	0.507
1.200	0.407	0.137	0.456
1.300	0.395	0.245	0.360
1.400	0.388	0.241	0.371

$\lambda(\mu m)$	$\rho(0,\lambda)$	ϵ_λ	τ_λ
1.450	0.327	0.285	0.388
1.500	0.331	0.287	0.382
1.600	0.351	0.221	0.428
1.800	0.368	0.226	0.406
2.000	0.338	0.496	0.166
2.500	0.236	0.568	0.196
3.000	0.019	0.981	0.000
4.000	0.091	0.851	0.058
5.000	0.134	0.687	0.179
6.000	0.019	0.981	0.000
7.000	0.022	0.978	0.000
8.000	0.018	0.982	0.000
9.000	0.026	0.974	0.000
10.000	0.024	0.976	0.000
12.000	0.031	0.961	0.008
14.000	0.019	0.981	0.000
16.000	0.025	0.975	0.000
18.000	0.020	0.980	0.000
20.000	0.016	0.984	0.000
22.000	0.017	0.983	0.000
24.000	0.042	0.958	0.000
25.000	0.003	0.997	0.000

REPORT DOCUMENTATION PAGE

Form Approved
OMB No. 0704-0188

1. AGENCY USE ONLY (Leave Blank)	2. REPORT DATE	3. REPORT TYPE AND DATES COVERED
	June 1992	

4. TITLE AND SUBTITLE

Data Analysis for Bark and Leaf Reflectance Measurements

5. FUNDING NUMBERS

C - F19628-89-C-0128
PE - 62101F
PR - 3054
TA - 2
WU - AJ

6. AUTHORS

J.H. Gruninger, D.C. Robertson, and M.M. Pervaiz

7. PERFORMING ORGANIZATION NAME(S) AND ADDRESS(ES)

Spectral Sciences, Inc., 99 South Bedford Street, #7, Burlington, MA 01803-5169

Phillips Laboratory, Hanscom AFB, MA 01731-5000
Contract Manager: Dean Kimball/GPOS

8. PERFORMING ORGANIZATION REPORT NUMBER

SSI-TR-197
PL-TR-92-2151

9. SPONSORING/MONITORING AGENCY NAME(S) AND ADDRESS(ES)

SWOE Program Office
U.S. Army Cold Regions Research and Engineering Laboratory
Hanover, New Hampshire 03755-1290

10. SPONSORING/MONITORING AGENCY REPORT NUMBER

SWOE Report 92-6

11. SUPPLEMENTARY NOTES

12a. DISTRIBUTION/AVAILABILITY STATEMENT

Approved for public release; distribution is unlimited.

12b. DISTRIBUTION CODE

13. ABSTRACT (*Maximum 200 words*)

This report addresses the incorporation of the effects associated with natural environments and backgrounds in the simulation models which are essential to the development of smart weapons. The effect of leaves and bark in the visible and IR spectral regions is discussed and a computational model is presented for the bi-directional reflectance (BRDF) measurement carried out by Surface Optics Corporation (SOC). A singular value decomposition (SVD) technique is used to justify an important model assumption, factorization of the spectral and angular dependencies into separate product functions. An empirical reflectance model, previously developed by Spectral Sciences, Inc. (SSI), is applied to these data. Since the leaves are translucent at shorter wavelengths, this model is expanded to include a very simple description of the directional transmittance.

14. SUBJECT TERMS

Measurements
Info Bases
IR Thermal Modeling
Radiance Modeling

15. NUMBER OF PAGES
54

16. PRICE CODE

17. SECURITY CLASSIFICATION OF REPORT	18. SECURITY CLASSIFICATION OF THIS PAGE	19. SECURITY CLASSIFICATION OF ABSTRACT	20. LIMITATION OF ABSTRACT
UNCLASSIFIED	UNCLASSIFIED	UNCLASSIFIED	Same as Report